TEKNILLINEN TIEDEKUNTA

INITIAL SLAG IN PRIMARY DESULPHURISATION OF HOT METAL

Pauli Pekuri

YMPÄRISTÖTEKNIIKAN TUTKINTO-OHJELMA

Diplomityö

Helmikuu 2020

TIIVISTELMÄ

Alkukuona raakaraudan primääririkinpoistossa

Pauli Pekuri

Oulun yliopisto, Ympäristötekniikan tutkinto-ohjelma

Diplomityö 2020, 97 s. + 2 liitettä

Työn ohjaajat yliopistolla: DI Tero Vuolio, TkT Ville-Valtteri Visuri

Raakaraudan primääririkinpoistoprosessin tehokkuus SSAB Raahen terästehtaalla vaihtelee suuresti. Tämän oletetaan johtuvan osittain siitä, että myös primääririkinpoiston alkukuonan määrän ja koostumuksen vaihtelu tehtaalla on suurta. Tämän työn päätavoitteena oli tutkia alkukuonan määrää ja koostumusta, sekä tunnistaa alkukuonan vaikutus primääririkinpoistoprosessiin. Toinen tavoite oli etsiä vaihtoehtoisia alkukuonanmuokkaajia kirjallisuusselvityksen avulla nykyisin käytössä olevan soodan tilalle.

Työn teoriaosassa on esitetty yleisimmät raakaraudan rikinpoistomenetelmät sekä kalkkipohjaisen reagenssi-injektion pääreaktiot ja -reaktiomekanismit. Raakaraudan rikinpoisto tapahtuu pääosin reagenssi-metalli-reaktiona, mutta tässä työssä tarkastelun pääpaino on metalli-kuona-reaktiossa. Lisäksi teoriaosaan on sisällytetty kirjallisuusselvitys vaihtoehtoisista alkukuonanmuokkaajista, joista potentiaalisimmilta vaikuttivat nefeliinisyeniitti sekä Na_2O-SiO_2-CaF_2-pohjaiset seokset.

Alkukuonan koostumuksen ja määrän tutkimiseksi järjestettiin näytteenottokampanja, jonka aikana kerättiin näytteitä alkukuonasta primääririkinpoistolaitoksella. Lisäksi järjestettiin koejakso, jonka aikana kokeiltiin jatkuvavaluprosessin kuonan hyödyntämismahdollisuutta alkukuonan muokkauksessa, sekä standardisoitiin alkukuonan koostumusta kuonalisäyksellä. Ennen koejaksoa arvioitiin kuonalisäyksen vaikutuksia alkukuonan sulaosuuteen, dynaamiseen viskositeettiin ja kuonan rikkikapasiteettiin. Koejakson tuloksia käyttämällä selvitettiin alkukuonan määrää ja lähteitä taselaskennan keinoin. Lisäksi kuonakomponenttien vaikutusta primäärikinpoistoon tutkittiin hyödyntämällä lineaarista monimuuttujaregressiomallinnusta. Kuonakomponenttien vaikutusta

rikinpoistotehokkuuteen ja raakaraudan loppurikkipitoisuuteen ei onnistuttu havaitsemaan muodostettujen mallien avulla.

Jäähdytetyn alkukuonapalan rakennetta ja mineralogista koostumusta tutkittiin ja sen pääfaasi identifioitiin lasifaasiksi, jonka koostumus oli lähellä meliliittiä. Pääfaasista oli erkaantunut larniittia dendriitteinä ennen näytteen jähmettymistä, mistä voidaan päätellä, että kuona oli näytteenottohetkellä sulaa. Tämä puolestaan viittaa siihen, että tämänhetkinen alkukuonanmuokkaaja oli toiminut tarkoituksessaan hyvin.

Työssä havaittiin, että lämpötila sekä kuonan CaO- ja Na_2O-pitoisuudet kasvattavat rikin jakaantumiskerrointa ja kuonan rikkikapasiteettia, mangaanin kuonassa pienentäessä niitä. Alkukuonan keskimääräisen massan arvioksi koejaksolla saatiin 480,6 kg. Noin puolet alkukuonan massasta arvioitiin olevan peräisin senkasta irronneesta skollasta, masuunikuonan osuuden ollessa arvioiden mukaan noin neljäsosa. Tehtyjen havaintojen perusteella alkukuona oli sulaa koejakson aikana. Kuonien rikkikapasiteetit laskettiin ja niitä verrattiin Youngin ym. (1992) esittämän mallin ennusteisiin. Mallin suorituskyky havaittiin olevan heikohko tällä aineistolla, jonka vuoksi rikkikapasiteetin ennustamiseen muodostettiin regressiomallinnusta käyttäen uusi malli. Malli suoriutui kohtuullisen hyvin tämän työn aineistolla eikä sisältänyt vaikeakäyttöisiä muuttujia.

Asiasanat: raakarauta, rikinpoisto, kuona

ABSTRACT

Initial Slag in Primary Desulphurisation of Hot Metal

Pauli Pekuri

University of Oulu, Degree Programme of Environmental Engineering

Master's thesis 2020, 97 pp. + 2 Appendixes

Supervisors at the university: Tero Vuolio, M.Sc. (Tech.), Ville-Valtteri Visuri, D.Sc. (Tech.)

The efficiency of the primary desulphurisation process at SSAB Europe Oy, Raahe steel plant varies greatly. This is assumed to be partly due to the fact that the amount and composition of initial slag in primary desulphurisation exhibit large variances. The main goal of this thesis was to study the composition and amount of initial slag, and to identify the effect of initial slag on the efficiency of the primary desulphurisation process. Another aim was to search for alternative initial slag modifying agents, to replace the currently used sodium carbonate, by means of a literature review.

In the theoretical part of the thesis, the most common methods for desulphurisation of hot metal are presented, as well as the main reactions and reaction mechanisms of the CaO-based reagent injection. The desulphurisation of hot metal occurs mainly as a reagent-metal reaction, but in this thesis the emphasis is on the slag-metal reaction. In addition, the theoretical part contains a literature review of alternative initial slag modifying agents, of which nepheline syenite and Na_2O-SiO_2-CaF_2-based agents seemed to be the options with the most potential.

In order to study the composition and amount of initial slag, a sampling campaign was organised, during which initial slag samples were collected at the primary desulphurisation plant. Additionally, an industrial test-run was conducted, during which the utilisation potential of ladle slag was tested in initial slag modification, and the composition of initial slag was standardised by a slag addition. The effects of the slag addition on the liquid fraction, dynamic viscosity and the sulphide capacity of the slag were estimated beforehand. The amount as well as the origin of initial slag were studied based on mass balance calculations utilising the data of the test-run. Moreover, the

effect of slag components on primary desulphurisation was studied by making use of multi-variable linear regression modelling. Unfortunately, the effect of slag components on desulphurisation characteristics, namely desulphurisation efficiency and the amount of sulphur in hot metal after desulphurisation, could not be identified.

The structure and mineralogical composition of a rapidly cooled piece of initial slag was investigated, and the main phase was identified to be a glassy phase with a composition close to that of melilite. From the main phase, a larnite phase had started to crystallise as dendrites before the sample had solidified. This result indicates that the slag sample was molten at the moment of sampling. Thus, the current initial slag modifying agent had successfully fluidised the slag.

It was discovered that the temperature as well as the amounts of CaO and Na_2O in the slag increase the sulphur distribution ratio and the sulphide capacity of the slag, whereas manganese in the slag decreases them. The obtained estimate for the average mass of initial slag during the test-run was 480.6 kg. With respect to the mass, around half of initial slag was estimated to be constituted of skull worn off the ladle, and around one-fourth was estimated to have originated from blast furnace slag. The initial slag during the test-run was liquid according to observations that were made. The sulphide capacities of the slags were calculated and compared to those estimated utilising a model proposed by Young et al. (1992). The performance of the model was found to be rather poor with the present dataset, thus a novel model for predicting the sulphide capacity of the slag was constructed using regression modelling. The model performed with reasonable accuracy using the present dataset and did not contain any complex parameters.

Keywords: hot metal, desulphurisation, slag

PREFACE

The work of this thesis was carried out while employed in the ironmaking process development group at SSAB Europe Oy, Raahe steel plant during 23.4.2019–23.10.2019. The main motive for commissioning this thesis was the uncertainties concerning the properties of the initial slag in primary desulphurisation of hot metal, and the effect of those on the efficiency of the primary desulphurisation process.

I would like to express my gratitude towards the supervisors of this thesis at the University of Oulu: Mr. Tero Vuolio and Dr. Ville-Valtteri Visuri, who provided a notable amount of guidance through the course of this work with their vast knowledge on the subject, and aided in the analysis of the results. I would also like to thank Dr. Ville-Valtteri Visuri for carrying out the FactSage-calculations that were incorporated in the work. In addition, I would like to thank the supervisor of the thesis at SSAB Europe Oy, Raahe, Dr. Antti Kemppainen, for assisting in organising the experiments conducted during the work.

I would like to express additional acknowledgements to Dr. Timo Paananen for offering me the opportunity to work with this subject, the specialised sampling group for collecting the samples, and the laboratory personnel for performing the corresponding analyses. I am also very grateful to my friends for allowing me to take my mind off the thesis at times, and to my family for enabling me to go through with my studies by providing their unconditional support.

Raahe, 6.2.2020

Pauli Pekuri
Pauli Pekuri

TABLE OF CONTENTS

NOMENCLATURE

Abbreviations

BF	blast furnace
HM	hot metal
PCI	pulverised coal injection
NST	nepheline syenite tailings
LS	ladle slag
SSE	sum of squared estimate of errors
MVLR	multi-variable linear regression
MAE	mean absolute error
VIF	variance inflation factor
HMD	hot metal desulphurisation
XRF	X-ray Fluorescence

Symbols

kg/tHM	kilograms per ton of hot metal
K	equilibrium constant
$a_{\mathrm{i}}^{\mathrm{R}}$	Raoultian activity of species *i*
$a_{\mathrm{i}}^{\mathrm{H}}$	Henrian activity of species *i*
S_{eff}	desulphurisation efficiency [%]
q	the specific consumption of the desulphurisation reagent [kg/tHM]
m_{HM}	mass of hot metal
$m_{\mathrm{CaO,inj.}}$	mass of injected CaO
M_{i}	molar mass of species *i*
$f_{\mathrm{i}}^{\mathrm{H}}$	Henrian activity coefficient of species *i*
$e_{\mathrm{i}}^{\mathrm{j}}$	interaction coefficient between species *i* and *j*
A_f	nominal slag-metal contact area [m^2]
k_f	mass transfer coefficient for the permanent contact reaction [m/s]
C_m^b	bulk uniform molar concentration of sulphur in metal [mol/m^3]
C_m^i	interfacial concentration of sulphur at the top slag metal interface [mol/m^3]
C_{S}	sulphide capacity of slag

P_i	partial pressure of species *i*
$f_{S^{2-}}$	activity coefficient of sulphur
L_S	sulphur distribution ratio
B	basicity
Λ	optical basicity
Λ_i	optical basicity of slag component *i*
k	number of components in the slag phase
$\hat{X}_i$	cation fraction of component *i*
n	number of oxygen atoms in a slag component
μ	dynamic viscosity of the slag [Pa·s]
μ_0	dynamic viscosity of the liquid part of the slag [Pa·s]
f	volume fraction of solids
$\propto$	maximum solid fraction of the slag
γ_i^R	Raoultian activity coefficient
x_i	molar fraction of species *i*
α	interaction energy between cations [J]
X	cation fraction
$\Delta G_{conv.}$	conversion energy of activity coefficient between a real solution and a hypothetical regular solution
T_0	temperature before desulphurisation [°C]
S_t	amount of sulphur in metal after desulphurisation [wt-%]
H_0	null hypothesis
H_a	alternative hypothesis
b_j	regression coefficient of explanatory variable *j*
α	confidence level
n	number of observations
k	number of explanatory variables
R^2	coefficient of determination
$R^2_{adj.}$	adjusted coefficient of determination
e_i	prediction error for datapoint *i*
R_j^2	coefficient of multiple determination obtained by regressing x_j on the other explanatory variables

Brackets

[ ]	species in metal phase
( )	species in slag phase
< >	species in solid phase
{ }	species in gas phase
$[\%S]_0$	amount of sulphur in metal before desulphurisation [wt-%]
[%S]	amount of sulphur in metal after desulphurisation [wt-%]
[%i]	weight percentage of species *i*

1 INTRODUCTION

Sulphur is typically one of the unwanted impurities in steel, although some steel grades include sulphur as an alloying element. Coke is the main source of sulphur in the blast furnace (BF) process as it contains around 0.5 wt-% sulphur. Normally, hot metal that leaves the BF contains 0.03 wt-% sulphur, but the requirement for the steel can be as low as 0.001 wt-%. Sulphur decreases the weldability and corrosion resistance of steel and increases its brittleness. For this reason, sulphur needs to be removed from the hot metal. (Schrama et al. 2017, p. 333)

Primary desulphurisation of hot metal is used as a pre-treatment method in iron ore-based steelmaking. At SSAB Europe Oy, the efficiency of the primary desulphurisation process has a large variance.

Slag plays an essential role in the hot metal desulphurisation process, because under reductive conditions of the process, slag captures sulphur mostly in the form of sulphides. It is only when the slag is skimmed off that sulphur is removed from the hot metal. (Schrama et al. 2018a) The composition and amount of initial slag in desulphurisation, i.e. the slag in the hot metal transfer ladle between the BF and the desulphurisation plant, varies greatly. One of the main hypotheses is that these properties of the initial slag may induce some variance to the overall efficiency of the process. However, the contributions of different mechanisms on the overall desulphurisation rate are difficult to distinguish in plant practice. This is due to the relative contributions of the transitory (reagent-metal) and permanent contact (slag-metal) reactions changing during powder injection (Chiang et al. 1990, p. 36), and the rate of the transitory reaction being typically the most significant single factor concerning the overall rate of reaction (Sawada 1986; Jin et al. 2006).

The aim of this thesis is to estimate the composition and amount as well as their variances of the initial slag in primary desulphurisation, and furthermore to identify the effect of initial slag on the efficiency of the primary desulphurisation process. The composition of initial slag was studied by conducting a sampling campaign at the primary desulphurisation plant. An industrial test-run was also carried out, during which

ladle slag was tested as an initial slag modification agent. The aim of the test-run was twofold: 1) to test an alternative initial slag modification agent, and 2) to standardise the composition of the initial slag by ladle slag addition.

Sodium carbonate is currently used as an initial slag modifying agent. It is added on the bottom of the ladles before hot metal tapping to decrease the melting temperature of the slag and to make it more fluid. This thesis contains a brief literature review on alternative materials for initial slag modification. One reason for the search for alternative initial slag modifying agents is the damage to ladle refractories caused by sodium carbonate.

2 HOT METAL DESULPHURISATION

Most steel plants worldwide use hot metal desulphurisation, because it is more process- and cost efficient to remove the sulphur before the converter. Primary desulphurisation at SSAB Raahe is conducted by injecting a lime-based reagent into the hot metal via a submerged refractory coated lance. A process flowchart of the steelmaking process from the BF to the converter is presented in Figure 1. Hot metal desulphurisation consists of two main reactions (Pal & Patil 1986, p. 294):

- **Transitory reaction:** reaction between the hot metal and reagent particles dispersed in the melt
- **Permanent contact reaction:** reaction between the hot metal and the top slag

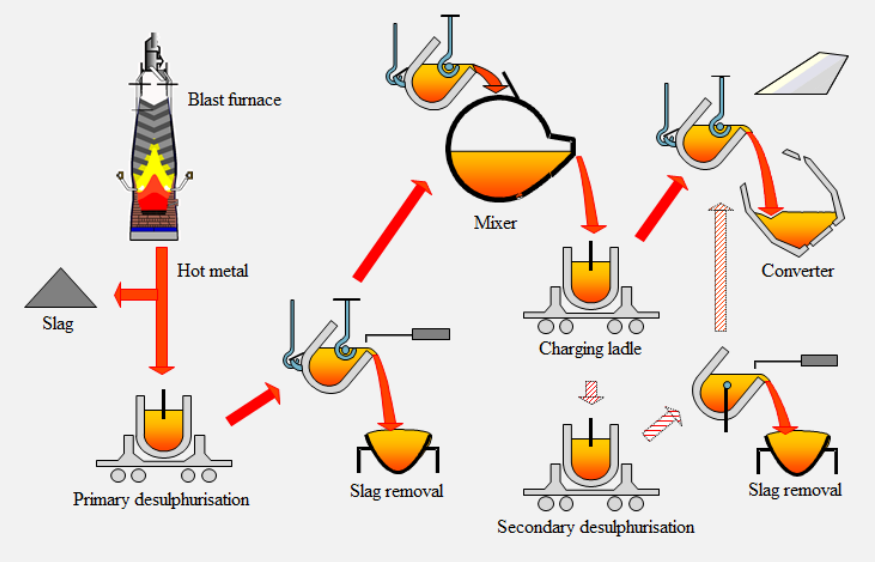

Figure 1. The steelmaking process from the BF to the converter (modified from SSAB 2015).

Hot metal desulphurisation is performed externally from the blast furnace and converter for the following reasons (Chiang 1986, p. 15):

- Higher sulphur operation of the BF increases the productivity and reduces the fuel rate at lower slag basicity
- For alkali removal in the blast furnace, low slag basicity is favourable

- The activity of dissolved oxygen in hot metal is low due to the high carbon and silicon content
- Desulphurisation can be more easily accomplished in hot metal, because the activity coefficient of sulphur in the hot metal is higher than that of sulphur in steel

2.1 Desulphurisation in blast furnace

The iron BF is a counter-current reactor, which produces hot metal out of iron ore, which is loaded in the process in the form of sinter or pellets. Full pellet operation is used at SSAB Raahe. Coke and pulverised coal injection (PCI) are used as reductants and fuels for heating. Iron-bearing materials, coke and limestone are charged alternately at the top where the materials flow downwards. Hot oxygen-enriched blast is blown through tuyeres, which are located at the lower part of the furnace. The hot blast produces BF gas, which ascends through the ore and coke layers, heating them up and reducing the ore. The melted ore is tapped at the bottom of the furnace. (Husslage 2004, p. 12)

In the BF, sulphur is released from the carbonaceous material and transferred to the gas phase. The sulphurous gas reacts with liquid metal, slag, and ferrous components and calcium compounds inside the BF. A major fraction of the sulphur is removed via slag-metal contact. Slag can desulphurise the metal in the dripping zone, the hearth, and during tapping. (Husslage 2004, p. 27) Sulphur transfers into the slag phase by means of formation of sulphides of Ca, Mg, Na and Mn, which are absorbed by slag. The chemical affinity of elements to sulphur increases in the following order: FeS < MnS < MgS < Na_2S < CaS. The main desulphurisation agents in BF are Ca and Mg. (Babich et al. 2008, p. 237–238) Slag is the main output of sulphur from the BF. Top gas and top dust account only for a few percent units of the sulphur output. Around 10% of sulphur exits the BF dissolved in the hot metal. (Husslage 2004, p. 19) The desulphurisation reaction in the BF is presented in Equation (1) (Husslage 2004, p. 46):

$$(\mathrm{CaO}) + [\mathrm{S}] + [\mathrm{C}] = (\mathrm{CaS}) + \{\mathrm{CO}\}, \quad (1)$$

where round brackets, square brackets and curly brackets designate a species in slag phase, metal phase and gas phase, respectively. Sulphur transfer from iron to slag as well as the accompanying iron and silicon transfer for a graphite saturated iron and $CaO\text{-}Al_2O_3\text{-}SiO_2$ slag is presented in Figure 2. It can be seen that the sulphur distribution between the tapped metal and slag are in apparent chemical equilibrium. This proposition is supported by data on quenched furnaces and other samples. This is the situation despite the fact that the metal and slag compositions may change during one cast. (Bakker et al. 2002, p. 4) Therefore, variance in the metal quality results from variations in the furnace conditions and the slag chemistry (Husslage 2004, p. 20). However, laboratory experiments conducted by Condo (2018) on re-melted samples of blast furnace hot metal and slag indicate that the two phases are not in equilibrium at tapping with respect to sulphur. Samples taken from BF no. 4 at SSAB Oxelösund were re-melted at 1743 K and 1773 K and stirred at 100 rpm for different lengths of time. From the plotted concentrations of sulphur in the hot metal and slag it was evident that the concentrations varied with time, indicating that the two phases where not in equilibrium at tapping with respect to sulphur.

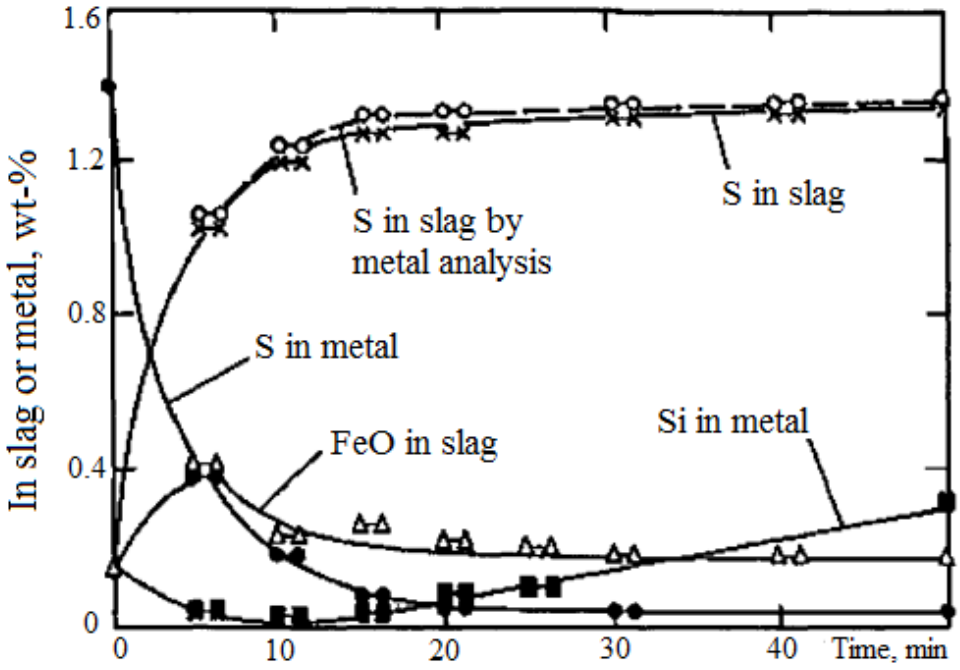

Figure 2. Sulphur transfer between metal and slag and the accompanying iron and silicon transfer for a graphite-saturated iron and $CaO\text{-}Al_2O_3\text{-}SiO_2$ slag. (modified from Husslage 2004, p. 47)

The volume of BF slag is closely linked with sulphur distribution between metal and slag. If the slag volume is reduced without improving sulphur distribution, there will be an increase in the sulphur content of the hot metal. Sulphur distribution depends on BF hearth conditions described above, and the sulphide capacity of slag. (Husslage 2004, p. 20) The sulphide capacity of slag is discussed later on in this thesis.

2.2 Methods for external desulphurisation of hot metal

The main reaction mechanisms of the powder injection desulphurisation processes are transitory contact (reagent-metal) and permanent contact (slag-metal) reactions. In desulphurisation in a torpedo ladle, the reagent is injected into the hot metal via a submerged lance. Nitrogen is typically used as a carrier gas. The reagent reacts with the sulphur in the metal, forming CaS or Na_2S, which ascend to the slag layer. A skimmer is then used to rake off the slag. Nowadays torpedo desulphurisation is mostly replaced by ladle desulphurisation, because the shape of torpedo cars caused very short contact

times and poor mixing, and the slag was difficult to remove. (Schrama et al. 2017, p. 337–338; Kitamura 2014, p. 189)

At SSAB Europe in Raahe there are three stages in which sulphur can be removed from hot metal: 1) blast furnace tapping, 2) primary hot metal desulphurisation, and 3) secondary hot metal desulphurisation. The principle of desulphurisation is to transfer the dissolved sulphur from the hot metal to the slag. After desulphurisation, the slag layer is removed on the top of the hot metal. A common technique for sulphur removal is the powder injection process, in which a suitable desulphurisation reagent is injected in hot metal via an immersed lance. The most used reagents are calcium carbide (CaC_2), magnesium (Mg) and burnt lime (CaO). (Schrama et al. 2017, p. 333–336)

In the co-injection hot metal desulphurisation process, both magnesium and fluidised lime or calcium carbide are injected into the hot metal. Co-injection uses the advantages of lime/calcium carbide (deep desulphurisation) and magnesium (faster process). In the literature, sulphur concentrations below 0.001 % (10 ppm) have been reported with magnesium/lime co-injection. A variation of this process is multi-injection, in which all three components are injected. The reagents are injected via a submerged refractory coated lance. An inert carrier gas (usually nitrogen) promotes mixing of the metal bath. In co-injection and multi-injection, the ratio of the reagents can be controlled accurately, because the reagents are injected from separate vessels and mixed in the injection line. (Schrama et al. 2017, p. 338–339)

The Kanbara reactor is a desulphurisation process developed by Nippon Steel in 1965 in Hirohata, Japan. The reactor uses relatively cheap coarse lime with 5–10 % CaF_2 or CaC_2 as a reagent, which is applied on top of the hot metal ladle in the first few minutes of the process. A submerged impellor is used for mixing the reagent with the hot metal at one-third of the bath depth. After 5–15 minutes of mixing the impellor is lifted and the bath is allowed to rest for 5–10 minutes, during which the slag and the formed CaS ascend to the top. After resting, the slag layer is skimmed off, as in other desulphurisation methods. With the Kanbara reactor, sulphur concentrations below 0.001 % (10 ppm) have also been reported in the literature. (Schrama et al. 2017, p. 339)

2.3 Slags in external desulphurisation of hot metal

Slags in ladle metallurgical processes have two purposes (Kingston & Caley 1989, p. 207):

1) to remove certain impurities from the hot metal, particularly sulphur and/or phosphorus, and
2) to protect the hot metal from the surrounding atmosphere.

Temperature and slag composition are important parameters affecting the assimilation of CaO by slags. The dissolution of CaO into the slag phase is a requirement for effective steelmaking practice. (Amini et al. 2007, p. 32) Amini et al. (2007) studied the dissolution of dense lime in molten slags at laboratory-scale at steelmaking temperatures. One of the results the authors obtained was that the dissolution of CaO is faster at higher temperatures. At 1500 °C, the authors detected a Ca_2SiO_4 layer, which hindered the dissolution of CaO. No Ca_2SiO_4 layer was observed in experiments with flux addition, which according to the authors was a major factor in explaining the increased rate of CaO dissolution into the slag phase.

2.3.1 Initial slag in primary desulphurisation of hot metal

The initial slag of hot metal desulphurisation is a multicomponent system, of which the oxide part is a Na_2O-CaO-SiO_2-Al_2O_3-MgO system. Usually the composition corresponds to BF slag, because slag and metal phases cannot be separated perfectly during the tapping. (Kitamura 2014, p. 183) Along with BF slag, the main constituents of the slag originate from the iron runner and ladle refractories. A part of the oxides are formed when Fe, Mn, Si, V and Ti in hot metal oxidise in the atmosphere contact. (Diao et al. 2009, p. 546)

Chiang (1986) studied hot metal desulphurisation by calcium carbide powder injection. Four types of initial slag conditions were used: no slag, dry slag, liquid slag and modified dry slag. The study indicated that the type of slag is of great importance to the rate and efficiency of desulphurisation. Liquid slag is favourable only when its sulphide capacity is high and the activity of oxygen is low in hot metal. According to the author,

the liquid slag with a low sulphide capacity could induce severe resulphurisation when the slag reaches its refining limit. However, if sufficiently high liquid slag volume is presented, the liquid slag can prevent the resulphurisation. When using no slag or dry slag as the initial slag condition, a 30- to 50-second incubation period was observed. This was explained by the author as sulphur reversion to the hot metal owing to low sulphide capacity of the slag and the high oxygen activity due to contact with the atmosphere. The incubation period can be eliminated by modifying the top slag with an addition of fluxes and slag compounds with high sulphide capacities.

2.3.2 Primary desulphurisation slag

From the primary desulphurisation plant, the ladles of hot metal are transported to the mixers, where the slag layer is removed. Therefore, the hot metal desulphurisation slag is also referred to as mixer slag at SSAB Europe Oy. After the skimming, the hot metal is poured into the mixers and the slag is transported to the slag mound, where it is poured and left to cool. The cooled slag is further transported to a plant where iron is separated from the slag. In 2008, around 86 000 tons of primary desulphurisation slag were produced. Around 6 000 tons were large skulls. Around 80 000 tons were processed in order to separate iron from the slag. (Hulkkonen 2009, p. 9–10)

According to Schrama et al. (2018a), initial slag from the BF contributes 60–80% of the total volume of the slag at the end of the hot metal desulphurisation process. However, calculations made by Palovaara (2013) and Vuolio (2017) suggest that this is not the situation at SSAB Europe Oy, Raahe. The results obtained by Vuolio (2017) indicate that the mass of the initial slag in desulphurisation exhibits significant variance. The lowest estimates for the mass of initial slag reported by Palovaara (2013) and Vuolio (2017) were 125 kg and 250 kg, respectively. The amount of injected reagent can be as high as 1 200 kg at the present time, which indicates that the contribution of initial slag to the composition of the primary desulphurisation slag can be much lower than estimated by Schrama et al. (2018a).

2.4 Desulphurisation at SSAB Raahe steel plant

2.4.1 Hot metal tapping at the blast furnaces

There are two nearly identical blast furnaces at the SSAB Raahe steel plant. Hot metal is tapped from the blast furnaces in two-hour cycles. The duration of a tapping is kept at 90 minutes, and between every tapping there is a 30-minute break. Sodium carbonate is added on the bottom or on the top of the ladle, based on the ladle filling practice. This is done in order to make the slag more liquid (Vuolio 2017, p. 64). The added amount of sodium carbonate is ~50 kg per ladle. The ladles are mainly filled starting from the north end of the ladles, when addition of sodium carbonate to the bottom of the ladle is easier.

During the tapping, every ladle of hot metal is sampled. The temperature of the hot metal is measured from the runner, first after one ladle of hot metal has been tapped, and again when the slag starts to exit the BF. After the tapping is complete, filled ladles are transported to the foundry via the desulphurisation plant and replaced with empty ladles from the foundry. The average measured properties of the hot metal are presented in Table 1 (modified from Palovaara 2013, p. 13; SSAB 2015).

2.4.2 Primary desulphurisation plant

At SSAB Raahe steel plant, sulphur is removed from the hot metal in a desulphurisation plant, which started operation in 1981. The desulphurisation is conducted by injecting powdery lime-based reagent into the hot metal through a submerged lance coated with refractory material. The carrier gas used is nitrogen. After the desulphurisation, the slag is removed from top of the hot metal before the hot metal is poured into the mixers. The sulphur content of hot metal is decreased from around 0.055 wt-% (550 ppm) to 0.008–0.012 wt-% (80–120 ppm). (SSAB 2015) Three factors are used to estimate the amount of reagent needed for the desulphurisation: 1) the amount of hot metal in the ladle, 2) sulphur content of the hot metal in the ladle, and 3) sulphur content of the hot metal in the mixers. The process flowchart can be seen in Figure 3 (modified from SSAB 2015).

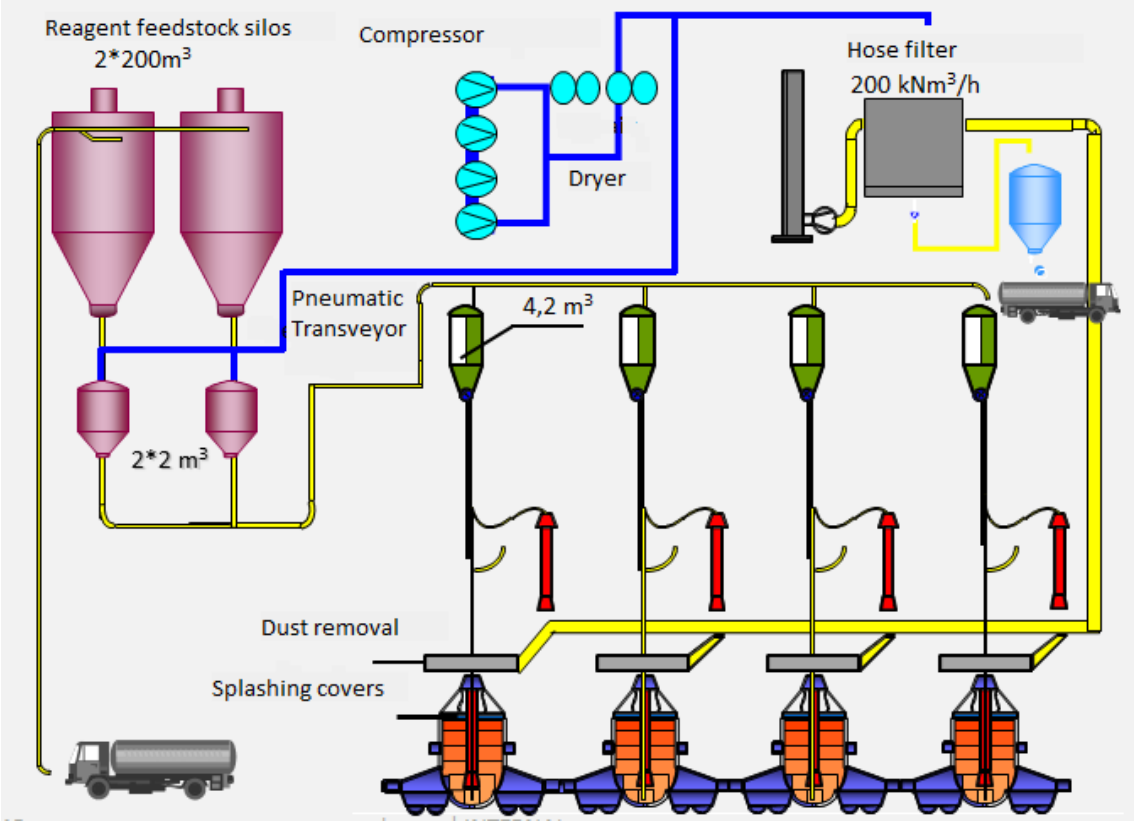

Figure 3. The process flowchart of the primary desulphurisation plant (modified from SSAB 2015).

The operation parameters of the desulphurisation plant are presented in Table 1 (modified from Palovaara 2013, p. 13; SSAB 2015). The injection parameters are difficult to change, because the flow rate cannot be controlled online. The feeding rate of the reagent is to some extent dependent on the injectability of the reagent. The only way at SSAB Raahe to adjust the feeding rate is to change the size of the nozzle in the bottom of the injection silo. With too low or alternatively excessively high feeding rates lance clogging becomes a problem, because the carrier gas is not able to keep the lance open. (Palovaara 2013, p. 13) In the study by Vuolio (2017), the injectability of a desulphurisation reagent was qualitatively attributed to reagent properties, namely to particle size distribution, density differences between the mixed compounds and to amount and quality of the used fluidising agent. Injection time is usually over 10 minutes. The factors affecting the injection time are the sulphur content of the hot metal in the ladle, the mass of the hot metal, and the mass flow rate of the reagent.

Table 1. The average operation parameters of the desulphurisation plant and average measured properties of the hot metal (modified from Palovaara 2013, p. 13; SSAB 2015).

Parameter	Value
Reagent input (varies between 80 and 120 kg/min)	100 kg/min
Carrier gas flowrate (NTP)	550 l/min
The pressure of carrier gas (absolute)	5.5 bar
Injection time	>10 min
Consumption of the reagent	>10 kg/tHM
Average sulphur content before desulphurisation	0.055 %
Average sulphur content in the hot metal in the mixers	0.008 – 0.012 %
Average temperature before desulphurisation	1350 °C
Average temperature after desulphurisation	1325 °C

Note: absolute pressure = static pressure + gauge pressure.

3 MODIFICATION OF INITIAL SLAG IN HOT METAL DESULPHURISATION

This chapter includes a brief literature review on different initial slag modifying agents used in primary desulphurisation of hot metal. While different fluxing agents, which are injected with the desulphurising agent, and the modification of post-desulphurisation slag have been the focus of several studies (Zhou 2012, Magnelöv et al. 2013, Yang et al. 2016, Schrama et al. 2018b), the modification of initial slag has drawn less attention.

3.1 Initial slag modifying agents

Slag modifying agents can be used with the injected reagent to fluidise the slag. Usually, the amount of hot metal entrapped in the slag decreases with the increase of liquid phase fraction of slag. Possible slag modifying agents include, e.g. dolomitic lime ($CaMg(CO_3)_2$), fluorspar (CaF_2), silica (SiO_2), potassium chloride (KCl), sodium chloride (NaCl), cryolite ($Na_3{\cdot}AlF_6$), potash, colemanite ($Ca_2B_6O_{11}{\cdot}5H_2O$), potassium cryolite ($KAlF_4$), calcium aluminates, calcium chloride ($CaCl_2$), sodium fluoride (NaF), nepheline syenite, anhydrous borax ($Na_2B_4O_7$) and sodium carbonate (Na_2CO_3). (Diao et al. 2009, p. 546)

3.1.1 Fluorspar (CaF_2)

The main component of fluorspar is CaF_2, a common slag modifying agent used to increase the dissolution of CaO into the slag. Although being an excellent fluidiser, CaF_2 has some negative effects which have hindered its use and have led to searching for alternative materials (Amini et al. 2007, p. 32; Walker 2010, p. 3; Kingston & Caley 1989, p. 208):

- CaF_2 causes emissions of hazardous fluoride species,
- it causes leaching of fluoride from generated slag,
- it causes refractory wear and its supplies are dwindling, and
- it is a relatively expensive industrial mineral.

Van Niekerk & Dippenaar (1993) studied Na_2O and CaF_2 containing CaO-based slags for desulphurisation of carbon-saturated hot metal. The results the authors obtained indicated that CaF_2 does not improve the desulphurising ability of liquid CaO-based slags. The sulphide capacity of Na_2O-SiO_2-CaO-CaF_2 slags decreases as a function of CaF_2 content of the slag. The authors attributed this to CaF_2 diluting the slag with respect to the amount of free oxygen ions. To avoid the detrimental effect on the sulphide capacity, only enough CaF_2 should be used to ensure that the slags are in liquid phase during the desulphurisation process.

3.1.2 Nepheline syenite

Nepheline syenite consists of three primary minerals: nepheline ($NaAlSiO_4$), albite ($(Ca,Na)(Al,Si)AlSi_2O_8$), and microcline ($KAlSi_3O_8$). Nepheline syenite is commonly used in the glassware industry. In the preparation of this mineral for industrial applications, the main beneficiation step is the removal of iron oxide, which is a common discolourant. The chemical composition of the resulting nepheline syenite tailings (NST) is approximately 50 wt-% SiO_2, 20 wt-% Al_2O_3, 10 wt-% FeO, 15 wt-% alkalines (Na_2O and K_2O), and minor amounts (5 wt-%) of various oxides, mainly CaO. (Tribe et al. 1994, p. 147)

Tribe et al. (1994) studied the replacement of fluorspar with NST as a slag modifying agent in secondary steelmaking. The authors carried out rheological tests, which indicated that NST slag could not reach as low values for viscosity as fluorspar slag. However, the difference was considered negligible. The compositions of the rheologically tested slags can be seen in Table 2. The NST slag solidified slower and over a wider temperature range than the fluorspar slag. Laboratory tests to study the attack on magnesia–carbon refractories indicated that the effect of NST slags is similar to fluorspar-containing slags. For the refractory tests, the slag compositions were modified to create a more fluid and less basic slag which provided a worst case scenario with respect to refractory corrosion. The compositions of the refractory-tested slags are presented in Table 2. Both of the tested slags penetrated into and reacted with individual magnesia particles located at the slag-refractory interface. For the fluorspar-containing

slag the penetration was indicated by the presence of F^- within the magnesia containing slag particles. In the case of NST slags, no such tracer ions, i.e. Na^+ or K^+, were found.

Table 2. The compositions of the rheologically and refractory-tested slags in wt-%.

Slag type	CaO	SiO_2	MgO	CaF_2	NST
Rheologically tested base slag	45.0	30.0	10.0	15.0	0
Rheologically tested NST slag	45.0	30.0	10.0	0	15.0
Refractory-tested base slag	40.0	35.0	10.0	15.0	0
Refractory-tested NST slag	40.0	35.0	10.0	0	15.0

3.1.3 Al-based initial slag modifying agents

While adding Al-based slag modifying agents to the hot metal before desulphurisation is done to achieve desired physical properties of the slag, limitations regarding the use still exist. Acidic Al_2O_3-SiO_2 based agents can be detrimental for desulphurisation due to reduced slag basicity. Also, the cost of the slag modifying agent is increased due to the high cost of aluminium powder. (Diao et al. 2009, p. 546–547)

3.1.4 Na_2O-SiO_2-CaF_2-based initial slag modifying agents

Diao et al. (2009) studied the effects of different slag modifying agents on desulphurisation using lime and magnesium co-injection. Their aim was to modify the post-desulphurisation slag, but the slag modifying agent was added prior to desulphurisation as in initial slag modification. The authors carried out laboratory scale experiments using crucibles and industrial tests with a 100 t transfer ladle containing 75–85 t hot metal by making use of five different slag modifying agent groups. During the industrial tests, 40–80 kg of slag modifying agent was added to the ladle before the desulphurisation. The agent that showed the best results contained 50.69 wt-% SiO_2, 21.15 wt-% Na_2O, 19.9 wt-% CaF_2, 5.74 wt-% CaO, and 2.53 wt-% Al_2O_3, and was applied for industrial production at Qingdao Iron and Steel Co., China. The slag modifying agent was found to have no negative effect on desulphurisation. In industrial tests, the average desulphurisation efficiency exceeded 82 % when using a desulphurisation reagent containing 80 wt-% CaO, 15 wt-% Mg and 5 wt-% CaF_2. The

reagent consumption was 3.5–4.0 kg/tHM and the average injection time was 5.4 minutes. The amount of slag modifying agent varied between 0.7 and 1.0 kg/tHM. The slag skimming time decreased from nearly 12 min to 6.5 min, and the heat loss during desulphurisation decreased from 34 °C to ~19 °C.

3.1.5 Summary

A summary of the properties and applicability of the initial slag modification agents discussed in this Section is provided in Table 3.

Table 3. Summary of the initial slag modifying agents.

Modifying agent	Advantages	Disadvantages
CaF_2	Excellent fluidiser, increases dissolution of CaO into the slag	Decreases the sulphide capacity, causes emissions of hazardous fluoride species, leaching of fluoride from generated slag and refractory wear, dwindling supplies, price
Nepheline syenite	Similar to CaF_2 in initial slag modification, but the slag solidifies slower	–
Al-based agents	–	Can reduce slag basicity, price
Na_2O-SiO_2-CaF_2-based agents	Successfully tested in industrial operation, decreased iron losses and slag skimming time	–

3.2 Effect of initial slag modification on the desulphurisation properties of slag

Initial slag modifying agents improve the fluidity of the slag by decreasing its melting temperature and viscosity (Diao et al. 2009, p. 546). Liquid slags are generally thought to have better desulphurisation properties than dry or solid slags (Holappa 1980, p. 262; Chiang 1986, p. 90; Kitamura 2014, p. 187–188). The effect of liquid slags may be attributed to the reaction kinetics due to increased rate of mass transfer at the slag-metal interface. However, for slags with high sulphide capacities the explaining factor could be the increase in the thermodynamic driving force. (Vuolio et al. 2019, p. 1792) Liquid slags have the ability to immediately dissolve the initial amount of CaS. In the study on hot metal desulphurisation by CaC_2 powder injection conducted by Chiang (1986), dry initial slag was found to have an incubation period, during which no desulphurisation was observed. No incubation period was observed for liquid slag or modified dry slag. (Chiang 1986, p. 90)

4 REACTIONS AND REACTION MECHANISMS

Effective desulphurisation is based on three factors: low oxygen content of the metal, reasonable slag fluidity, and high slag basicity (Wolfe & Olson 2003). Desulphurisation by slag via an ion exchange reaction is shown in Equation (2), where the free oxygen ion is dissolved in the slag phase (Kitamura 2014, p. 180):

$$[\mathrm{S}] + (\mathrm{O}^{2-}) = (\mathrm{S}^{2-}) + [\mathrm{O}]. \tag{2}$$

The equilibrium constant for Equation (2) is:

$$K_2 = \frac{a^{\mathrm{R}}_{(\mathrm{S}^{2-})} a^{\mathrm{H}}_{[\mathrm{O}]}}{a^{\mathrm{H}}_{[\mathrm{S}]} a^{\mathrm{R}}_{(\mathrm{O}^{2-})}}, \tag{3}$$

where K_2 is the equilibrium constant of Equation (2), and $a_{\mathrm{i}}^{\mathrm{R}}$ and $a_{\mathrm{i}}^{\mathrm{H}}$ are the Raoultian and Henrian activities of species *i*, respectively. The equilibrium constant suggests that the sulphur partition ratio between slag and hot metal phases can be increased by: increasing the activity of sulphur, and decreasing the activity of oxygen in metal, whereas an increase in the activity of oxygen ions in the slag and a small sulphur content in the slag promote the desulphurisation reaction. (Kitamura 2014, p. 180)

4.1 Main reactions

Equation (4) shows the desulphurisation reaction with CaO (Wolfe & Olson 2003):

$$(\mathrm{CaO}) + [\mathrm{S}] = (\mathrm{CaS}) + [\mathrm{O}]. \tag{4}$$

The equilibrium constant for the reaction is:

$$K_4 = \frac{a^{\mathrm{R}}_{(\mathrm{CaS})} a^{\mathrm{H}}_{[\mathrm{O}]}}{a^{\mathrm{R}}_{(\mathrm{CaO})} a^{\mathrm{H}}_{[\mathrm{S}]}}. \tag{5}$$

For effective levels of desulphurisation, the activity of CaO in the slag phase should be as high as possible (Wolfe & Olson 2003).

When sodium carbonate or soda ash (Na_2CO_3) is added to hot metal, it decomposes into Na_2O and CO_2 according to Equation (6) (Pak & Fruehan 1987, p. 687):

$$(Na_2CO_3) = (Na_2O) + \{CO_2\}. \quad (6)$$

Other possible reactions are decarburisation according to Equations (7)–(8), oxidation of silicon by Na_2CO_3 and Na_2O according to Equations (9)–(10), and desulphurisation by Na_2O according to Equation (11).

$$(Na_2CO_3) + 2\,[C] = 2\,\{Na\} + 3\,\{CO\} \quad (7)$$

$$(Na_2O) + [C] = 2\,\{Na\} + \{CO\}, \quad (8)$$

$$(Na_2CO_3) + [Si] = (SiO_2) + 2\,\{Na\} + \{CO\} \quad (9)$$

$$2\,(Na_2O) + [Si] = (SiO_2) + 4\,\{Na\}, \quad (10)$$

$$(Na_2O) + [S] + [C] = (Na_2S) + \{CO_2\}. \quad (11)$$

The evaporation of Na produces a strong flare and fume. The resulting slag from a sodium carbonate treatment is a Na_2O-SiO_2-based slag containing sulphur, phosphorus, and possibly some Na_2CO_3, among other species. (Pak & Fruehan 1987, p. 687–688)

Even though the process using sodium carbonate is simple, the desulphurising ability is low. The disadvantages of the sodium carbonate process are the danger of attack on the ladle refractories, low desulphurisation efficiency when sodium carbonate is added to the bottom of the ladle, and health hazard due to alkali fumes. (Babich et al. 2008, p. 243) Most of the desulphurising ability of sodium carbonate is lost at iron and steelmaking temperatures due to its low boiling point (Kanyangarara 1982, p. 22). Studies found in the literature indicate that increase in Na_2O content of the slag increases the sulphide capacity of the slag (Inoue & Suito 1982; Chan & Fruehan 1989;

Van Niekerk & Dippenaar 1993; Sano 2003; Cho et al. 2010) and thus increases the desulphurisation rate (Tong et al. 2017; Choi et al. 2001). The Na_2O-equivalent of CaO was defined by Van Niekerk & Dippenaar (1993) as 0.30. The role of Na_2O in the slag is to increase the activity of dissolved CaO (Vargas-Ramirez et al. 2001, p. 177). Owing to its low boiling point, the amount of Na_2O in the slag has been found to decrease with time due to evaporation (Choi et al 2001). The evaporation rate has been found to increase with increasing temperature and slag basicity (Li et al. 2015).

In calcium carbide injection technologies, calcium carbonate ($CaCO_3$) is usually added to the reagent as a gas releasing agent. $CaCO_3$ decomposes to CaO and CO_2 at ~850 °C thus generating large amounts of gas. (Irons 1989, p. 32) A premature suggestion made by Irons and Farias was that $CaCO_3$ decomposition promotes mixing of the hot metal bath and particle-liquid contact (Irons & Farias 1986, p. 306). However, the effect of $CaCO_3$ on the rate of desulphurisation via mixing has been proven negligible, as the reaction is hardly ever controlled by mixing of the metal bath. The beneficial effect of $CaCO_3$ is to provide more interfacial area for the bubbles on which the reagent particles reside. (Irons 1989, p. 35) The effect of $CaCO_3$ on the kinetics of the transitory reaction on an industrial-scale was quantified by Vuolio et al. (2018). On the other hand, Zhao (1992) demonstrated that $CaCO_3$ is detrimental for CaC_2 desulphurisation due to formation of CO_2, because low oxygen activity is required for effective desulphurisation. However, it should be noted that the activity of oxygen is important when the sulphur content is near the thermodynamic equilibrium. Primary desulphurisation operates far from the thermodynamic equilibrium. Another problem addressed by Zhao is the strong endothermic decomposition reaction of $CaCO_3$, which lowers the temperature of the hot metal bath. (Zhao 1992, p. 258) The decomposition reaction of $CaCO_3$ is shown in Equation (12) (Halikia et al. 2001, p. 92):

$$\langle CaCO_3 \rangle \rightarrow \langle CaO \rangle + \{CO_2\}, \tag{12}$$

where angle brackets indicate solid species.

4.2 Desulphurisation efficiency

Different ways to calculate the desulphurisation efficiency have been presented in the literature (Shevchenko et al. 1984; Palovaara 2013; Vuolio 2017). One way to express desulphurisation efficiency is given in Equation (13):

$$\mathrm{S_{eff}}(\%) = \frac{[\%\mathrm{S}]_0 - [\%\mathrm{S}]}{[\%\mathrm{S}]_0} \times 100, \tag{13}$$

where $\mathrm{S_{eff}}$ is desulphurisation efficiency, $[\%\mathrm{S}]_0$ is the sulphur content before desulphurisation (wt-%), and [%S] is the sulphur content after desulphurisation (wt-%). The value of $\mathrm{S_{eff}}$ does not describe the effectiveness of the utilised desulphurisation reagent thoroughly. Thus, different ways to express desulphurisation efficiency are often considered. (Vuolio 2017, p. 29) Shevchenko et al. (1984) introduced the expression for a specific degree of desulphurisation:

$$\mathrm{S_{eff-d}}(\%) = \frac{[\%\mathrm{S}]_0 - [\%\mathrm{S}]}{[\%\mathrm{S}]_0 q} 100 \frac{(\%)}{\mathrm{kg/tHM}}, \tag{14}$$

where q is the specific consumption of the desulphurisation reagent (kg/tHM). The efficiency of the CaO in the reagent can be calculated by solving Equation (15):

$$\mathrm{S_{CaO,eff}}(\%) = \frac{m_{\mathrm{HM}}([\%\mathrm{S}]_0 - [\%\mathrm{S}])}{m_{\mathrm{CaO,inj.}}} \cdot \frac{M_{\mathrm{CaO}}}{M_{\mathrm{S}}}, \tag{15}$$

where m_{HM} is the mass of the hot metal (kg), $m_{\mathrm{CaO,inj.}}$ is the mass of the injected CaO (kg), and M_i is the molar mass of species i (kg/mol).

4.3 Transitory contact reaction

The transitory reaction of lime-based reagents is shown in Equation (4). It is often considered that the transitory reaction follows first-order reaction kinetics. This is based on the assumption that the control of the reaction rate is related to mass transfer. (Vuolio et al. 2018, p. 2693)

It is thought that the reaction rate of solid lime is controlled by the following steps (Kitamura 2014, p. 186):

- mass transfer of sulphur in hot metal,
- mass transfer of sulphur in solid lime, and
- mass transfer of sulphur in the layer of calcium sulphide formed on the lime surface.

The surface area of the fine particles injected into the hot metal is much larger than the metal-slag interfacial area. Because of this, the reactions in the rising gas-particle-liquid plume are potentially much faster than the reactions in the metal-slag interfacial area. However, short contact times or no contact time at all results in low reagent efficiencies and slow refining times. (Irons 1986, p. 3) Chushao & Xin (1992) investigated the effect of transitory and permanent contact reaction on sulphur removal rate with a kinetic model. In their research, hot metal contained 0.08 wt-% sulphur and 0.34 wt-% vanadium. The study indicated that the transitory reaction has an important role in desulphurisation during powder injection. Vargas-Ramirez et al. (2001) studied hot metal pre-treatment with lime-based reagents at laboratory scale. The authors conducted experiments during which reagent was injected at the beginning, after 11 minutes, and after 22 minutes, for one minute at a time. Desulphurisation, desiliconisation and decarburisation rates were considerably faster during the injection periods, indicating that the contribution of the transitory reaction during powder injection is more important than that of the permanent contact reaction. The authors suggested that possible reasons for the lower efficiency of the permanent contact reaction are the relatively short reaction time and the low reaction area between the hot metal and the slag. The importance of the transitory reaction in powder injection processes for pre-treatment of hot metal is recognised also by other studies found in the literature (Sawada 1986; Jin et al. 2006).

4.4 Activities of species in hot metal

4.4.1 Activity of sulphur in hot metal

The activity of sulphur in hot metal is strongly dependent on the composition of hot metal (Kitamura 2014, p. 180). For low solute contents, the activity of species *i* in hot metal is defined by Henry's law, where the activity of the species *i* approaches unity as the weight percentage of the component approaches zero (Turkdogan 1996, p. 91):

$$a_{\mathrm{i}}^{\mathrm{H}} = f_{\mathrm{i}}^{\mathrm{H}}[\%\mathrm{i}], \tag{16}$$

where $f_{\mathrm{i}}^{\mathrm{H}}$ is the Henrian activity coefficient and [%i] is the weight percentage of species *i*. The Henrian activity coefficient can be calculated using WLE-formalism (Sigworth & Elliott 1974):

$$\log f_{\mathrm{i}}^{\mathrm{H}} = \sum_{j=1}^{n_j} e_{\mathrm{i}}^{\mathrm{j}}[\%j], \tag{17}$$

where $e_{\mathrm{i}}^{\mathrm{j}}$ is the interaction coefficient between species *i* and *j*. The interaction coefficients used in this study were obtained from Sigworth & Elliott (1974) and are presented in Table 4. It can be seen from the table that C and Si increase the activity coefficient of sulphur, whereas Mn, V, Ti and O decrease it.

Table 4. Mass-based first-order interaction coefficients in liquid iron (Sigworth & Elliott 1974).

j	[Mn]	[V]	[Ti]	[Si]	[S]	[C]	[O]
$e_{[\mathrm{Si}]}^{\mathrm{j}}$	0.002	0.025	-	34,5/T+0.089	0.056	380/T-0.023	-0.23
$e_{[\mathrm{S}]}^{\mathrm{j}}$	-0.026	-0.016	-0.072	0.063	233/T-0.153	0.11	-0.27

4.4.2 Activity of oxygen in hot metal

As Equation (3) suggests, low oxygen activity in metal is favourable for desulphurisation, which has been confirmed in the case of CaC_2 desulphurisation by Zhao (1992). Another result obtained by the author was that the activity of oxygen prior

to powder injection is controlled by the [Si]/(SiO_2) equilibrium. This is the case for typical operating conditions, but the activity of oxygen can also be controlled by the oxidation of carbon. The reason for these controlling factors is that the activities of oxygen at equilibrium and in the metal bath differ greatly from each other. Thus, the reaction with the highest oxygen affinity can be used in determination of the equilibrium activity of oxygen. (Visuri et al. 2019, p. 33) In this work, the equilibrium activity of oxygen was determined by the [Si]/(SiO_2) equilibrium using Equation (18) (Visuri et al. 2019, p. 33):

$$\log a^{\mathrm{H}}_{[\mathrm{O}],[\mathrm{Si}]-(\mathrm{SiO_2})} = 5.698 - \frac{15053}{T} - 0.5 \log a^{\mathrm{H}}_{[\mathrm{Si}]} + 0.5 \log a^{\mathrm{R}}_{(\mathrm{SiO_2})}. \qquad (18)$$

4.4.3 Oxidation of silicon from hot metal

Si is most stable in oxidised form in oxidising atmosphere and ambient pressure and will thus easily oxidise when in contact with the atmosphere. Oxidation occurs readily at iron- and steelmaking temperatures. (Næss 2013, p. 8) The equilibrium of Si between the metal and the slag phase can be written as (Abd Elmomen 2017, p. 29):

$$[\mathrm{Si}] + \mathrm{O_2} = (\mathrm{SiO_2}). \qquad (19)$$

Goldman et al. (1954) studied the effects of different alloying elements on sulphur transfer from carbon-saturated iron to the slag phase and discovered in their experiments that SiO_2 always reduced from acid slags into the metal phase at a constant rate regardless of the silicon content of the metal, whereas Si oxidised from the metal phase into basic slags (Kanyangarara 1982, p. 25–26).

5 PERMANENT CONTACT REACTION

As discussed earlier, the permanent contact reaction occurs between the hot metal and the slag layer at each time instant when the slag is in contact with the hot metal. Although the transitory reaction plays a more important role in the desulphurisation process, studies found in the literature suggest that desulphurisation can be carried out via the permanent contact reaction (Ohguchi 1983; Chushao & Xin 1992).

5.1 Overall rate

The permanent contact reaction occurs very fast and the thermodynamic equilibrium will be achieved almost immediately at the slag-metal interface because of the high temperature of the hot metal in the ladle. The overall rate of the permanent contact reaction depends on the following factors (Cao et al. 2018, p. 990):

- the mass transfer rate of species to the slag-metal interface,
- chemical reaction rates at the slag-metal interface, and
- the mass transfer rate of the reaction products away from the slag-metal interface.

If the mass transfer of sulphur in the metal is assumed to be the rate controlling step, the rate of the permanent contact reaction can be written as (Deo & Grieveson 1988, p. 265):

$$-\frac{dC_m^b}{dt} = A_f k_f (C_m^b - C_m^i), \tag{20}$$

where A_f is the nominal slag-metal contact area, k_f is the mass transfer coefficient for permanent contact reaction, C_m^b is the bulk uniform molar concentration of sulphur in the metal, and C_m^i is the equilibrium interfacial concentration of sulphur at the top slag metal interface.

5.2 Kinetic and thermodynamic preconditions

The equilibrium between sulphur in the metal and in the slag phase depends on the following factors (Husslage 2004, p. 48):

- The temperature. The temperature affects the activities of the metal and the slag species, and the Gibbs free energy and thus the equilibrium of the reaction. Efficient desulphurisation is promoted by higher temperatures (Kitamura 2014, p. 184).
- The partial pressures of O and CO, which affect the activity of oxygen in the metal and slag phases.
- The activity of O in the slag and metal phases, which is a function of slag basicity. The sulphide capacity of high basicity slags, which contain many free O^{2-} ions, is higher than that of low basicity slags.
- The activities of sulphur in the slag and metal phase, and
- The presence of Fe^{2+} and Mn^{2+} in the slag phase, which are detrimental for desulphurisation, and Mn and Si in the metal phase, which promote desulphurisation. The desulphurisation power of the slag will be limited by Fe^{2+} and Mn^{2+} in the slag, unless they are reduced by a stronger deoxidiser.

As in the case of the transitory reaction, the permanent contact reaction is also generally thought to follow first-order reaction kinetics with respect to sulphur. The results obtained by Chiang (1986) support this suggestion. In order to obtain a high rate for the permanent contact reaction, it is favourable to (Chiang 1986, p. 40–41):

- increase the slag basicity,
- lower the oxygen potential,
- improve the stirring of the bath, and to
- avoid the existence of reducible oxides in the slag.

It can be assumed that for deoxidised hot metal with high slag basicity, the reaction rate of the permanent contact reaction is controlled by the transport kinetics in the hot metal (Chiang 1986, p. 40–41).

5.3 Sulphide capacity and sulphur distribution ratio of slag

Sulphide capacity designates the potential of a molten slag to remove sulphur. Being a property of the slag, sulphide capacity depends only on the temperature and the slag compositions. The sulphide capacity can be used to evaluate the desulphurisation characteristics of different slags. (Wang et al. 2018, p. 90) Sulphide capacity is presented in Equation (22) and is based on the reaction shown in Equation (21) (Kitamura 2014, p. 182):

$$\frac{1}{2}\mathrm{S}_2(\mathrm{g}) + (\mathrm{O}^{2-}) = \frac{1}{2}\mathrm{O}_2(\mathrm{g}) + (\mathrm{S}^{2-}) \tag{21}$$

$$C_{S^{2-}} = \frac{(\%S)\times \mathrm{P}_{O_2}^{1/2}}{\mathrm{P}_{S_2}^{1/2}} = \frac{a_{O^{2-}}}{f_{S^{2-}}} \times K_{21}, \tag{22}$$

where $\mathrm{P_i}$ is the partial pressure of species *i* and $f_{S^{2-}}$ is the activity coefficient of sulphur. This definition for sulphide capacity is based on the slag/gas equilibrium reaction. Sulphide capacity can also be defined based on the slag/metal equilibrium reaction, which is presented in Equation (4). K_4 and K_{20} are related via a metal/gas exchange reaction shown in Equation (23) (Moosavi-Khoonsari & Jung 2016, p. 2876):

$$\frac{1}{2}\{\mathrm{S}_2\} + [\mathrm{O}] = [\mathrm{S}] + \frac{1}{2}\{\mathrm{O}_2\} \tag{23}$$

$$K_{23} = \frac{a_{[\mathrm{S}]}^{\mathrm{H}}}{a_{[\mathrm{O}]}^{\mathrm{H}}} \left(\frac{p_{\mathrm{O}_2}}{p_{\mathrm{S}_2}}\right)^{\frac{1}{2}} \tag{24}$$

The sulphur distribution ratio of a slag is defined simply as the (slag)/[metal] ratio of sulphur as shown in Equation (25) (Kitamura 2014, p. 183). Studies found in the literature indicate that the sulphur distribution ratio can be improved by increasing the amount of the basic compound CaO in the slag with respect to intermediate and acidic ones (Andersson et al. 2000; Zhang et al. 2018; Wu et al. 2018; Varanasi et al. 2019). At lower basicity and thus lower CaO content of the slag, less free oxygen ions exist in the slag, thus leading to formation of SiO_2 networks. As the basicity of the slag increases, the networks are broken into smaller groups of anions, leading to an increase in the

proportion of free oxygen ions and thus the sulphur distribution ratio and the sulphide capacity. (Wu et al. 2018, p. 2027) Silicate networks and slag basicity are discussed in the next Section.

$$L_{\mathrm{S}} = \frac{(\mathrm{wt{-}\%\ S})}{[\mathrm{wt{-}\%\ S}]}, \tag{25}$$

where L_{S} is the sulphur distribution ratio. A relation between the sulphur distribution ratio and sulphide capacity can be obtained by rearranging Equations (22) and (24) (Moosavi-Khoonsari & Jung 2016, p. 2876):

$$\log_{10} C_{\mathrm{S}} = \log_{10} \frac{(\mathrm{wt{-}\%\ S})}{[\mathrm{wt{-}\%\ S}]} + \log_{10} a^{\mathrm{H}}_{[\mathrm{O}]} + \log_{10} K_{23} - \log_{10} f_{\mathrm{S}}. \tag{26}$$

In this work, the sulphide capacities of slags were calculated by solving Equation (26), in which the value of the equilibrium constant was approximated as follows (Zhu et al. 2016, p. 1371):

$$\log K_{23} = -\frac{935}{\mathrm{T}} + 1.375. \tag{27}$$

Numerous theoretical or semi-empirical models have been developed for predicting the sulphide capacity of the slag phase, of which the ones that are the most referred to are evaluated in Vuolio et al. (2019). The theoretical models focus on describing the effect of chemical interactions between the slag ions and molecules, and semi-empirical models use data-driven fitting techniques, i.e. the multiple linear regression or artificial neural networks in identifying the effect of system properties and slag composition on the sulphide capacity. Semi-empirical models often make use of the optical basicity concept to elucidate the interactions between the slag composition, system properties, and sulphide capacity. (Vuolio et al. 2019, p. 1793) An expression for optical basicity of the slag is presented in Equation (28) (Sosinsky & Sommerville 1986, p. 332):

$$\Lambda = \sum_{i=1}^{k} \Lambda_i \hat{X}_i, \tag{28}$$

where Λ is optical basicity, k is the number of components in the slag phase, Λ_i is the optical basicity of slag component i, and $\hat{X}_i$ is the cation fraction of the corresponding component. The cation fractions of the slag components can be calculated using Equation (29) (Sosinsky & Sommerville 1986, p. 332):

$$\hat{X}_i = \frac{nx_\mathrm{i}}{\sum_{i=1}^{k} nx_\mathrm{i}}, \tag{29}$$

where x_i is the molar fraction of slag component i and n is the number of oxygen atoms in the corresponding component. A model proposed by Young et al. (1992) uses the optical basicity, temperature, and weight percentages of some slag components for calculating the sulphide capacity of the slag phase. Regardless of simplifications and inconveniencies in the formulation of the model, the performance of the model is reasonably good when assessed with an external data set (Vuolio et al. 2019, p. 1794). The equations for sulphide capacity are (Young et al. 1992, p. 212):

$$\log C_\mathrm{S} = -13.913 + 42.84\Lambda - 23.82\Lambda^2 - \frac{11710}{T} - 0.02223(\mathrm{wt-\%\ SiO_2}) - 0.02275(\mathrm{wt-\%\ Al_2O_3}), \Lambda < 0.8 \tag{30}$$

$$C_\mathrm{S} = -0.6261 + 0.4808\Lambda + 0.7197\Lambda^2 + \frac{1697}{T} - \frac{2587\Lambda}{T} + 0.0005144(\mathrm{wt-\%\ FeO}), \Lambda \geq 0.8. \tag{31}$$

Sulphide capacity does not elucidate the effects of different slag components on the activities of sulphur and oxygen ions. For example, the sulphide capacity observed for manganese silicates is higher than that of calcium silicates. However, the activity of MnS is very much lower than the activity of CaS, when the SiO_2 content is constant, and sulphur partitioning decreases as lime is substituted with MnO. (Kanyangarara 1982, p. 19)

Schrama et al. (2018a) performed calculations using FactSage 7.1 to evaluate the influence of slag composition and temperature on the sulphide capacity. They used typical composition of the BF slag at Tata Steel IJmuiden, the Netherlands, in their calculations. It is notable that the slag contained only wt-0.4 % Na_2O, and that initial

slag and BF slag have different compositions. The results showed that for the typical BF slag composition around 39 wt-% CaO, the single-phase liquid is stable only above 1350 °C. The sulphide capacity decreases and the solid fraction increases with decreasing temperature. Increase in solid fraction leads to increased effective viscosity and thus more iron droplet entrapment in slag.

5.4 Slag basicity

Slag basicity is an indirect measure for the number of network breakers in the slag and is used as an indicator to describe the slag structure. Some oxide components of slag form complexes with O^{2-} anions; these acceptor oxides are called acid components of slag. Some components, e.g. CaO, do not form complexes with O^{2-} anions and are ionic in nature. These donor oxides are called basic components of slag. Some oxides, e.g. Al_2O_3, can act both as an acceptor oxide and donor oxide. These components are called amphoteric. (Husslage 2004, p. 43)

Slag polymerisation is mainly induced by silicates in BF slags. In silicate slags, four O^{2-} anions are surrounding the Si^{4+} cations. Together these constitute a tetrahedral SiO_4^{4-} unit structure. Several O^{2-} anions are shared by adjacent tetrahedrons, depending on the SiO_2 content of the slag, forming rings or chains. Large polymerised ions can form in this manner. The degree of polymerisation affects the properties of slag, such as slag viscosity. A high slag viscosity is a result of a high degree of polymerisation. (Husslage 2004, p. 43)

Slag basicity is often presented as the ratio of possible network breakers to network formers. The simplest approximation of slag basicity is shown in Equation (32) (Husslage 2004, p. 44). The slag basicity has an important effect on the amount of sulphur which can be incorporated into a slag. An O^{2-} ion is replaced by a S^{2-} ion when sulphur is incorporated in a slag. Basic slags contain many free O^{2-} ions and are ionic in nature. In acid slags the oxygen is bound in networks or complexes, which are difficult to enter by sulphur. This is because of the fact that the sulphur ion is much larger than the oxygen ion. Therefore, basic slags are more suitable for desulphurisation than acid slags. (Husslage 2004, p. 44) One of the main difficulties regarding the use of basic

slags is that basic oxides, e.g. CaO and MgO, have very high melting points. Because of this, fluxes must be added to reduce the slag's liquidus temperature to an appropriate level for iron- and steelmaking. (Walker 2010, p. 10–11)

$$\mathrm{B} = \frac{\text{wt}-\%\ \mathrm{CaO}}{\text{wt}-\%\ \mathrm{SiO_2}}, \tag{32}$$

where B is basicity of slag. The problem with this kind of expressions for basicity is that they are designed for the compositions of molten slags. In plant operation, the steelmaking slags often contain undissolved CaO and MgO. Without the correction for undissolved CaO and MgO, the analyses of such slags will give higher basicities than in the molten part of the slag. (Turkdogan 1996, p. 141)

The concept of optical basicity was defined by Duffy and Ingram (1976). They noticed that the number of free O^{2-} in a slag can be measured by a frequency in the UV frequency region. The optical basicity of a slag is given by Equation (33) and is usually related to that of CaO as the standard. Values of optical basicity for some common oxides are presented in Table 5. Of these oxides, BaO and CaO are considered basic and SiO_2 and P_2O_5 are considered acid. The rest of the oxides are classified as intermediate. (Husslage 2004, p. 43–44)

$$\Lambda = \frac{\text{electron donor power of slag}}{\text{electron donor power of CaO}}. \tag{33}$$

Table 5. Optical basicities of some common oxides relevant to iron- and steelmaking slags (Husslage 2004, p. 44).

Oxide	BaO	CaO	MnO	FeO	MgO	Al_2O_3	TiO_2	SiO_2	P_2O_5
Optical basicity	1.15	1.00	0.59	0.51	0.78	0.61	0.61	0.48	0.40

According to Kanyangarara (1982, p. 75), acid to base ratio is not a reliable measure of the desulphurising power of a slag. The reason for this is that different oxides have different degrees of acidity or basicity, and interactions between different slag components must be considered. The author conducted laboratory-scale experiments on desulphurisation of iron by different slags in a vertical molybdenum wire-wound

furnace. As a part of the study, three types of ilmenite ore were added to the slag phase: Norwegian, WMS and WSL. Although having the most favourable acid to base molar ratio, the Norwegian ilmenite ore had lower desulphurisation efficiency when compared to the WMS ore which had a higher acid to base ratio. The author explained the better performance of the WMS ore by the difference in the SiO_2 content of the ores. The lower SiO_2 content in the WMS ore outweighed the beneficial effect of a higher FeO content in the Norwegian ore.

5.5 Viscosity of slag

In steelmaking, viscosity of a slag is a factor affecting the separation between metal and slag phases. Viscosity defines the motion of a fluid in relation to applied stresses. (Walker 2010, p. 11)

Convective mass transfer can be a rate-limiting step in slag-metal reactions. Thus, the slag must be sufficiently fluid for significant convection to occur, and for the slag-metal reactions to occur in a reasonable amount of time. (Walker 2010, p. 11) Low viscosity slags are favourable also because lower levels of slag viscosity result in lower iron losses during slag skimming, in particular the emulsion loss, wherein the metal droplets are emulsified in the slag phase. However, the quantitative relation between slag viscosity and emulsion loss has not been found yet, because slag viscosity and emulsion loss are challenging to measure in practice in steel plants. Estimated viscosities of slags vary greatly from 0.3 to 15 Pa·s. (Schrama et al. 2018a)

The Einstein-Roscoe equation, which is presented in Equation (34), is used to determine the viscosity of slags that are mostly liquid but contain a significant fraction (up to 5% or even 10%) of solid particles (Schrama et al. 2018a). The equation may prove impractical in estimating the viscosity of initial slag, which generally contains larger amounts of solid particles.

$$\mu = \mu_0(1-\propto\times f)^{-n}, \tag{34}$$

where μ is the dynamic viscosity of the slag, μ_0 is the dynamic viscosity of the liquid part of the slag (neglecting the influence of possible solid particles in the slag), *f* is the volume fraction of solids, $\propto$ is the maximum solid fraction of the slag, and *n* is a constant. (Schrama et al. 2018a)

Schrama et al. (2018a) calculated the effect of temperature on the dynamic viscosity of liquid slag (μ_0) and volume fraction of solids (*f*) on FactSage. Typical BF slag from Tata Steel IJmuiden, the Netherlands, was used. Large changes in viscosity and solid fraction were seen in the typical temperature range for hot metal desulphurisation (1250–1450 °C). For temperatures below 1392 °C, the solid fraction of the slag was above 10%. The viscosity of liquid slag is not relevant for the slag viscosity at these levels of solid fractions, so the viscosity was determined by the solid fraction only. In temperatures above 1400 °C the solid fraction was negligibly small.

5.6 Activities of slag species

The activity of species *i* in a metallurgical slag can be expressed using Raoult's law (Turkdogan 1996, p. 16):

$$a_i = \gamma_{\mathrm{i}}^{\mathrm{R}} x_{\mathrm{i}}, \tag{35}$$

where $\gamma_{\mathrm{i}}^{\mathrm{R}}$ is the Raoultian activity coefficient of species *i*. Thermodynamic activities of oxides dissolved in molten slags are relative to pure solid or liquid oxides as the standard state. Thus, for pure oxide the activity a_{MO} = 1. (Turkdogan 1996, p. 150) In this study, the Raoultian activity coefficients of the slag species were calculated using the regular solution model proposed by Ban-Ya (1993):

$$RT\ \ln\gamma_i = \sum_j \alpha_{ij} X_j^2 + \sum_j \sum_k (\alpha_{ij} + \alpha_{ik} - \alpha_{jk}) X_j X_k + \Delta G_{i,\mathrm{conv.}}, \tag{36}$$

where α is the interaction energy between the cations, *X* is the cation fraction, and $\Delta G_{conv.}$ is the conversion energy of activity coefficient between a real solution and a hypothetical regular solution. The values of α and $\Delta G_{conv.}$ are available in Ban-Ya (1993).

5.7 Resulphurisation of hot metal

The thermodynamic calculations conducted by Pal & Patil (1986) suggested that although the contribution of the transitory reaction is more important to desulphurisation, the equilibrium sulphur content is often higher for the permanent contact reaction. This indicates that a thermodynamic driving force exists for the inverse desulphurisation reaction, which is referred to as resulphurisation. (Vuolio et al. 2019, p. 1791)

The rate of resulphurisation is thought to be controlled by mass transfer in the slag phase. Thus, the rate of resulphurisation is controlled by the sulphide capacity of the slag through the thermodynamic driving force. The precondition for resulphurisation to occur is that the sulphur distribution ratio at time instant *t* is significantly higher than the sulphur distribution ratio at slag-metal equilibrium. (Vuolio et al. 2019, p. 1792)

6 EXPERIMENTAL PROCEDURE

A sampling campaign was conducted to obtain information concerning the composition and amount of the initial slag in primary desulphurisation. A further scope of this work is to identify the effect of initial slag on the efficiency of the primary desulphurisation. During the industrial test-run, ladle slag (LS) was tested as an alternative for sodium carbonate in initial slag modification.

6.1 Sampling campaign

Samples were taken from hot metal and slag before desulphurisation, and from hot metal after desulphurisation. The temperature of hot metal was measured at the same stage as the sampling by using a sampling probe which was equipped with a temperature sensor. The initial slag was sampled with a dipper. The sample was poured on a metal plate to cool down, after which it was crushed with a hammer and collected in a vessel. The hot metal was sampled manually.

Measurement of the thickness of the slag layer was attempted with a specially designed tool, which had a metal plate and two rods on its tip. The idea was to immerse the rods in the hot metal in order to get the metal to stick on them. The thickness of the slag layer could thus have been calculated as the length of the parts of the rods with no metal stuck to them. Unfortunately, it was found that the hot metal did not stick to the rods and consequently, further thickness measurements were cancelled.

6.2 Calculation of the amount of the ladle slag addition for the industrial test-run

In order to decide the amount of LS addition during the industrial test-run, the slag modifying effect of LS on the initial slag had to be studied. First, the compositions of the LS added slags were calculated based on the analyses of both slags. Calculations were made for different amounts of initial slag and LS. The calculated compositions of the resulting slags were then used to estimate liquid fractions and dynamic viscosities of

the slags using FactSage. A liquid slag with a low viscosity would be the most ideal for the subsequent desulphurisation of hot metal. In addition, sulphide capacities for the slags were calculated based on a model proposed by Young et al. (1992).

6.2.1 Estimation of the mass of the initial slag

Since the measurement of the thickness of the initial slag layer did not succeed during the sampling campaign, the mass of the initial slag was estimated based on previous estimations by Palovaara (2013) and Vuolio (2017). The estimated values ranged from 126 to 1480 kg. It should be noted that there is a large variance among the estimated values, and that there are many uncertainties concerning the system. The uncertainties in the calculations include, e.g., ignorance of the splashing of the slag, the possibility of non-representative samples, and the fact that a large amount of the injected reagent ends up in the dust-removal system during the injection (Vuolio 2017, p. 137).

Palovaara's work contained three and Vuolio's work 14 estimated values for the mass of the initial slag. Palovaara estimated the mass of the initial slag (Palovaara 2013, p. 107):

- with the aid of the mass of the Si transferred to the slag phase,
- with the aid of the mass of Al_2O_3, and
- by removing the masses of slag forming material and dispersed metal droplets from the mass of the slag removed at the mixers. The mass of the desulphurisation slag after desulphurisation was thus assumed to be constant, because the average mass of the removed slag was used.

Vuolio estimated the mass of the initial slag by mass balance calculations based on the analyses of the hot metal and slag samples before and after desulphurisation. The amounts of injected CaO and the sulphur extracted from the hot metal were considered to fully transfer to the slag phase. Other components were calculated based on the derived mass balance equations. (Vuolio 2017, p. 137)

6.2.2 Composition

The composition of the initial slag after LS addition was calculated based on the masses and analyses of both slags. The analyses of the slags are presented in Table 6 for LS addition and in Table 7 for Na_2CO_3 & LS addition. Normalised compositions of the slags were used. Different cases were calculated with varying amounts of both slags. The mass of the initial slag in the calculations varied between 100 and 1500 kg in 50 kg intervals. The average of the previous estimations, 586 kg, was also used. Amounts of added LS used in the calculations were 0, 20, 40, 60, 120, 160, 200, 300 and 400 kg.

Table 6. The compositions of the slags used in the case of LS addition (in wt-%).

	Na_2O	MgO	Al_2O_3	SiO_2	CaO	Fe	S	Sum
Initial slag (raw)	1.8	0.5	3.9	20.9	15.4	39.5	1.4	83.4
Initial slag (normalised)	2.16	0.60	4.68	25.06	18.47	47.36	1.68	100
LS (raw)	0.10	5.85	27.48	5.66	43.44	1.59	0.25	84.4
LS (normalised)	0.12	6.94	32.57	6.71	51.49	1.88	0.30	100

Table 7. The compositions of the slags used in the case of Na_2CO_3 & LS addition (in wt-%), where IS refers to initial slag.

	K_2O	Na_2O	S	MgO	Al_2O_3	SiO_2	CaO	Ti	Mn	Fe	Sum
IS (raw)	0.12	11.87	2.63	1.24	4.60	31.16	30.15	1.59	0.51	16.05	99.9
IS (norm.)	0.12	11.88	2.63	1.24	4.60	31.19	30.18	1.59	0.51	16.07	100
LS (raw)	0.16	0.10	0.25	5.85	27.48	5.66	43.44	0.53	0.70	1.59	85.8
LS (norm.)	0.19	0.12	0.29	6.82	32.05	6.60	50.66	0.61	0.81	1.85	100

6.2.3 Liquid fraction

The liquid fractions were calculated using the Equilib -module in FactSage at temperatures of 1300, 1350 and 1400 °C and a pressure of 1 atm. In the calculations, the FactPS -database for pure substances and the FToxid -database for oxides were employed. The gas phase was assumed to be ideal. In some cases, the results showed an area of two liquid phases. In these cases, the total liquid fraction was obtained by the sum of the two liquid phases. Estimated liquid fractions for the slags when the mass of the initial slag (m_0) is 200, 586 and 1400 kg and when no Na_2CO_3 is added are

presented in Figure 4 as a function of LS addition. It can be deduced from the figure that 40 and 60 kg LS additions seem the most suitable for obtaining a liquid slag in different cases, i.e. with different masses of the initial slag.

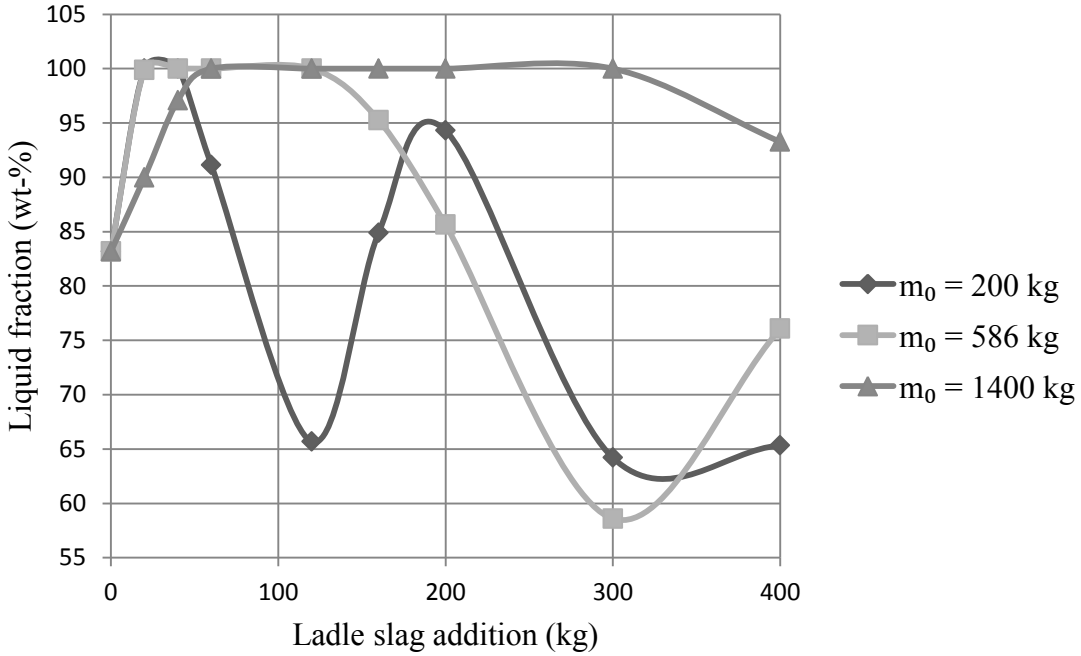

Figure 4. Estimated liquid fractions for the slags as a function of LS addition in 1350 °C when no Na_2CO_3 is added.

6.2.4 Dynamic viscosity

The dynamic viscosities were calculated for the liquid fractions using the Viscosity module of FactSage at temperatures of 1300, 1350 and 1400 °C. In Figure 5, the dynamic viscosities of the slags in 1350 °C when the mass of the initial slag is 200, 586 and 1400 kg and when no Na_2CO_3 is added are presented. It can be seen from the figure that dynamic viscosity of the liquid phase decreases as a function of LS addition. The effect of LS on the dynamic viscosity is more prominent when the added amount is larger compared to the total mass of the slag, i.e. when the mass of the initial slag is low. The viscosity curve decreases more steeply at low amounts of LS addition, suggesting that with a 40–60 kg addition, a reasonable modification to the dynamic viscosity of the slag would be obtained.

According to Schrama et al. (2018a), the viscosity of the liquid fraction of the slag is negligible when the solid fraction exceeds 10%. Thus, the results must be compared to the estimated liquid fractions. It can be seen from Figure 4 that with a 40–60 kg addition, the liquid fraction exceeds 90 wt-% with all three studied masses of initial slag. Therefore, with this amount of LS addition, a desired modification to the dynamic viscosity of the slag would be obtained.

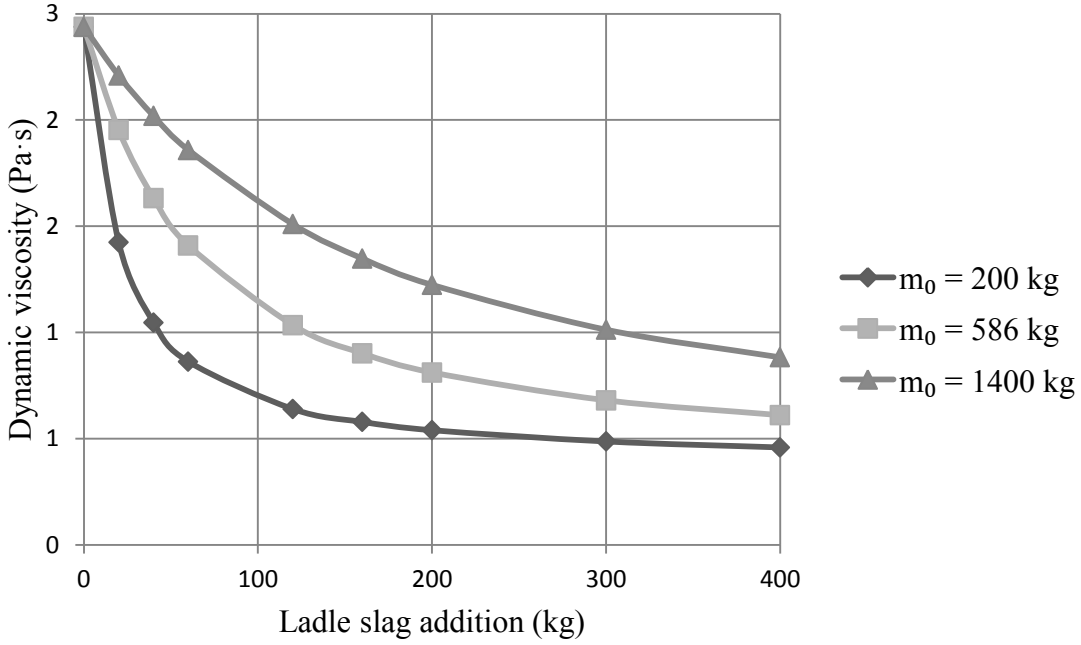

Figure 5. Dynamic viscosities of the liquid fractions of the slags in 1350 °C when the mass of the initial slag is 200, 586 and 1400 kg and no Na_2CO_3 is added.

6.2.5 Sulphide capacity

To further investigate the slag modifying effect of LS, sulphide capacities for the slags were calculated. A model proposed by Young et al. (1992) was chosen, because it seemed sufficiently accurate for the needs of the present study. The values for optical basicities of the slag components were obtained from Sosinsky & Sommerville (1986).

The values employed for the calculations represent three cases: a small amount of initial slag (200 kg), an average amount of initial slag (586 kg), and a large amount of initial slag (1400 kg), based on the previous estimations. Sulphide capacities of the slags as a function of LS addition in 1350 °C are presented in Figure 6. The temperature chosen

for the calculations is the average temperature of hot metal before desulphurisation. It can be seen from the figure that sulphide capacity increases as a function of LS addition. The effect is more prominent when no Na_2CO_3 is added, because slag with Na_2CO_3 addition has substantially larger sulphide capacity to begin with. However, in the case of no Na_2CO_3 addition, a large amount of LS would be needed to obtain a slag with equally high sulphide capacity when compared to Na_2CO_3 addition only.

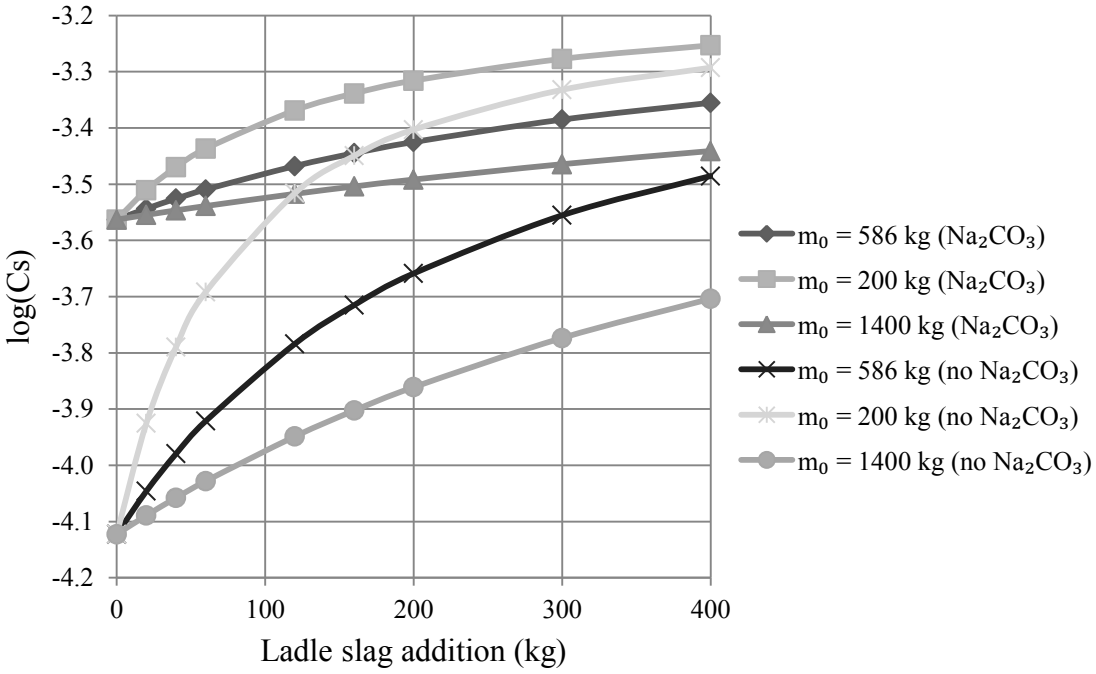

Figure 6. Calculated sulphide capacities of the slags as a function of LS addition in 1350 °C.

To study the effect of temperature, sulphide capacities of the slags in 1300 and 1400 °C were calculated. Sulphide capacities of the slags in different temperatures when the mass of the initial slag is 586 kg are presented in Figure 7. The figure shows the temperature-dependency of sulphide capacity. In the typical hot metal temperature of 1350 °C before desulphurisation, 300 kg of LS would be required for the slag without Na_2CO_3 addition to reach the same value of sulphide capacity as the slag with Na_2CO_3 addition only.

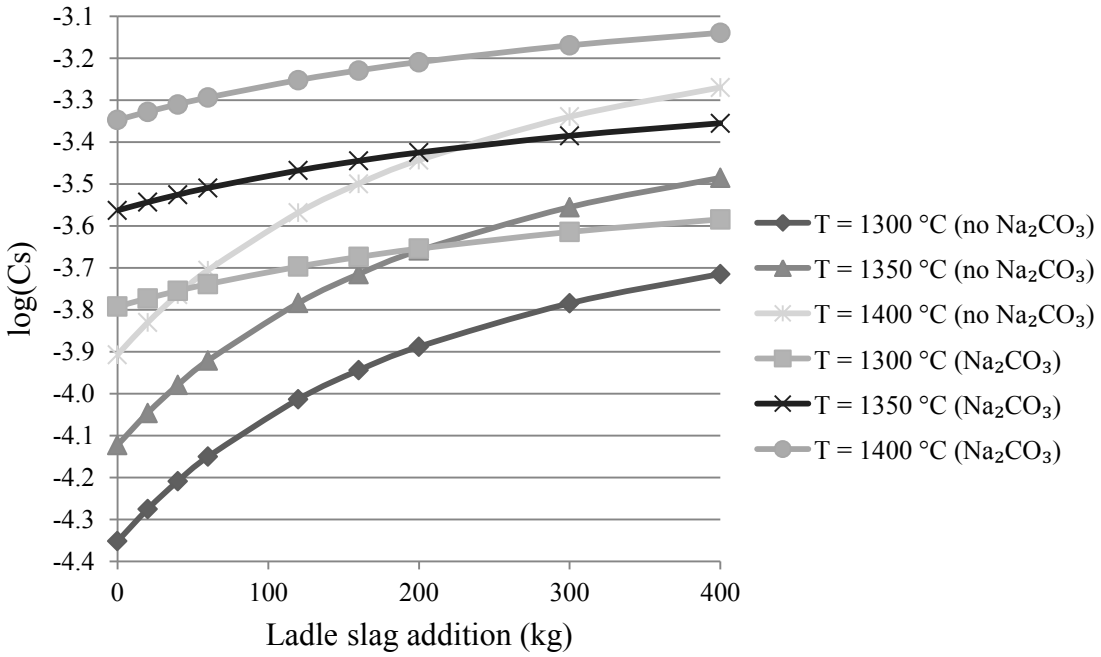

Figure 7. Calculated sulphide capacities of the slags in 1300, 1350 and 1400 °C when the mass of the initial slag is 586 kg.

The results obtained from the sulphide capacity calculations seem promising, since LS addition increases the sulphide capacity of the slag. This is mainly because of the fact that the nominal composition of the slag contains higher amounts of basic compounds (CaO) with respect to acid or intermediate ones (SiO_2, Al_2O_3). Based on the results of calculations of liquid fractions, dynamic viscosities and sulphide capacities, the amount of LS during the test-run was set to 50 kg.

6.3 Industrial test-run

During the test-run, both Na_2CO_3 and LS, and LS alone were tested. 50 kg of LS was added manually on the bottom of the empty ladles in 10 kg bags. In the case of Na_2CO_3 addition, LS was added before Na_2CO_3. Samples were taken at the primary desulphurisation plant from slag and hot metal before and after desulphurisation. Again, the temperature of the hot metal was measured simultaneously with the sampling.

A different method for sampling of the initial slag was successfully tested during the test-run. The tool was equipped with a metal plate which was immersed in the melt. The

purpose was to get the slag to stick on the plate. After sampling, the tool was left to cool down, after which the slag was separated from the tool, crushed with a hammer and collected in a vessel. The post-desulphurisation slag was sampled with a dipper.

6.3.1 Mass of the initial slag

The mass of the initial slag was approximated based on the predicted and measured slag compositions during the test-run. The study was conducted separately for the cases of LS addition and LS & Na_2CO_3 addition. Averages of the measured slag compositions were used in both cases. The LS used during the test-run was sampled, and its composition is shown in Table 8. This composition was used in the calculations.

Table 8. The composition of the ladle slag used during the test-run, in wt-%.

	Na_2O	MgO	Al_2O_3	SiO_2	CaO	S	Sum
Raw	0.17	5.80	28.91	13.69	44.21	0.23	93.01
Normalised	0.18	6.24	31.08	14.72	47.54	0.25	100

First, the sum of squared estimate of errors (SSE) was calculated for each individual case, i.e. for the predicted composition with varying mass of the initial slag. This value was then minimised utilising the Solver tool in MS Excel by changing the mass of the initial slag. The GRG Nonlinear module was utilised in the calculations, and the convergence criteria was set to 10^{-12}.

6.3.2 Origin of the slag components

The origin of the slag components was studied based on analyses of the main constituents of initial slag, namely BF slag, skull formed in the ladle, and the LS and Na_2CO_3 added to the ladle. Refractory wear was excluded from the study, because it was assumed to make the calculations more complex, since it is very unlikely that the refractories dissolve homogeneously into the slag phase. The Na_2CO_3 was assumed to be pure. Analyses of the skull in the ladle were obtained from Palovaara (2012). The amount of Si oxidised during the tapping was also evaluated based on hot metal samples taken at the BF and at the desulphurisation plant. It was assumed that the Si removed from the hot metal in the ladle between the blast furnace and the desulphurisation plant

completely oxidised to SiO_2 and transitioned to the slag phase. The mass of hot metal for each treatment was used to obtain the mass of the oxidised Si, and the average estimated mass of initial slag, 586 kg, was removed from the mass of the hot metal. In case of an increase in the Si content of the hot metal, it was assumed that the Si had transferred from the slag to the metal phase via a redox reaction. Mass balance equations were written for the slag components, and the masses of BF slag and skull were solved using an iterative approach by minimising the SSE for predicting the composition of the initial slag.

6.4 MVLR modelling

Multi-variable linear regression (MVLR) analysis was applied to analyse the results of the experimental campaigns. The response variables of interest were the desulphurisation efficiency (S_{eff}), the amount of sulphur in hot metal after desulphurisation (S_t) and the sulphide capacities of the slags (C_S). The primary aim was to identify the effect of slag composition on these.

Different groups of explanatory variables were tested, and the applicability of the variables was evaluated based on a two-tailed *t*-test. The postulated hypotheses were as follows (Rawlings et al. 1998, p. 17):

- H_0 (null hypothesis): the explanatory variable has no effect on the response variable ($b_j = 0$)
- H_a (alternative hypothesis): the explanatory variable has an effect on the response variable ($b_j \neq 0$),

where b_j is the regression coefficient for explanatory variable j. In multi-variable regression analysis, the regression coefficient b_j (also called partial regression coefficient) reflects the change in the response variable per unit change in the jth explanatory variable, assuming all other explanatory variables are held constant. The estimates of each regression coefficient depend on the set of explanatory variables in the model. (Rawlings et al. 1998, p. 76–77) That is, the regression coefficient b_j may be

used to estimate the effect of explanatory variable *j* given that the other explanatory variables are selected correctly (Montgomery et al. 2012, p. 121).

When testing the significance of a single explanatory variable in a MVLR model, the regression coefficients are usually evaluated with a *t*-test. In this test, the postulated null hypothesis ($b_j = 0$) can be rejected, if the P-value is lower than the chosen risk level (α). (Montgomery et al. 2012, p. 88) The P-value shows the probability of wrongly rejecting the null hypothesis. A small P-value is evidence that the explanatory variable explains the variation in the response variable, and thus the null hypothesis can be safely rejected. (Polychronopoulou et al. 2011, p. 22) The confidence level used in this study was $\alpha = 0.05$. In the two-tailed *t*-test, the null hypothesis is accepted if $P \geq \alpha$, and consequently rejected if $P < \alpha$ (Vasilopoulos 2011, p. 102).

Occasionally regression coefficients may have the wrong sign (+/-), which can be in conflict with previous knowledge on the effect of the particular explanatory variable on the response variable (Montgomery et al. 2012, p. 119). Mullet (1976) has pointed out that the wrong sign of the regression coefficient may be due to the following reasons (Montgomery et al. 2012, p. 119):

- the variance in the values of the explanatory variables are high, and the data has not been treated accordingly,
- important explanatory variables have not been included in the model or are not measured,
- there is multicollinearity between the explanatory variables, or
- computational errors have been made.

One way to measure the contribution of the explanatory variables in the model is the coefficient of determination (R^2). It ranges from zero to one, meaning that when R^2 approaches 1 (·100 %), most of the variation in the response variable is explained by the explanatory variables. (Rawlings et al. 1998, p. 9–10) In this work, the value of adjusted R^2, $R^2_{\text{adj.}}$ was used. $R^2_{\text{adj.}}$ is a rescaling of R^2 by degrees of freedom. It is an indicator that is more comparable than R^2 over models with different numbers of explanatory variables. Contrary to R^2, $R^2_{\text{adj.}}$ does not necessarily increase when variables are added

to the model. As the number of variables increases, $R^2_{\text{adj.}}$ tends to stabilise around some upper limit. The best model is chosen as the simplest model with $R^2_{\text{adj.}}$ near the upper limit. (Rawlings et al. 1998, p. 222–223) In this work, the error of each model was estimated by making use of mean absolute error (MAE) (Willmott & Matsuura 2005, p. 80):

$$\text{MAE} = \frac{1}{n}\sum_{i=1}^{n}|e_i|, \tag{37}$$

where n is the number of observations and e_i is the prediction error for datapoint i. Sometimes models are said to suffer from lack of fit (LOF), which indicates that important parameters that help describing the variance in the response variable have not been fitted in the model (Montgomery et al. 2012, p. 156).

Multicollinearity is a problem concerning regression models in which a near-linear dependency exists among the explanatory variables. When this is the situation, the use of the model may lead to misleading or incorrect deductions. The Variance Inflation Factor (VIF) measures the combined effect of the dependencies among the explanatory variables on the variance of a single explanatory variable. One or more large VIF values in the model are an indication of multicollinearity. (Montgomery et al. 2012, p. 296) Some commonly used thresholds for multicollinearity are VIF = 4 and VIF = 10 (O'Brien 2007, p. 684). The VIF values are calculated from the correlation matrix of the explanatory variables. Therefore, the explanatory variables are standardised to unit length and centred. The VIF values are obtained from the diagonal elements of the inverse of the correlation matrix. (Rawlings et al. 1998, p. 372) The simplest presentation for VIF value is as follows (Montgomery et al. 2012, p. 118):

$$\text{VIF}_j = \frac{1}{1-R_j^2}, \tag{38}$$

where VIF_j and R_j^2 are the VIF value and the coefficient of multiple determination obtained by regressing x_j on the other explanatory variables, respectively.

7 RESULTS OF THE SAMPLING CAMPAIGN

In this chapter, the results of the sampling campaign are presented and discussed. During the sampling campaign, 10 initial slag samples were collected. Box plots were used to detect outliers in the samples. Four samples were excluded from the results due to substantially high amounts of carbon. One sample was excluded due to the mass of hot metal not being available. The average composition of the initial slag during the sampling campaign is presented in Table 8 along with the average temperature before desulphurisation. The aforementioned samples were excluded from this data.

Table 9. The average composition of the initial slag during the sampling campaign (wt-%).

T_0 (°C)	K_2O	Na_2O	S	MgO	Al_2O_3	SiO_2	CaO	Fe	B (CaO/SiO_2)
1367	0.10	13.97	1.41	0.67	4.02	21.28	17.93	40.98	0.67

The data were combined with the analyses of 18 samples collected previously by Vuolio (2017). One of these samples was excluded from the analysis due to a low temperature.

7.1 Effect of temperature on the slag components

The weight percentages of the slag components were plotted as a function of temperature. Prior to this Fe was removed, and the compositions were normalised to 100%. The effect of temperature on the amount of CaO in the slag is presented in Figure 8. There are two possible reasons for the behaviour of CaO as a function of temperature: 1) The formation of SiO_2 is an exothermic reaction and thus at higher temperatures the amount of SiO_2 in the slag is lower. Due to this, the amount of the other main component becomes higher. 2) At higher temperatures the amount of CaO-bearing skull that wears off the ladle walls into the slag is higher.

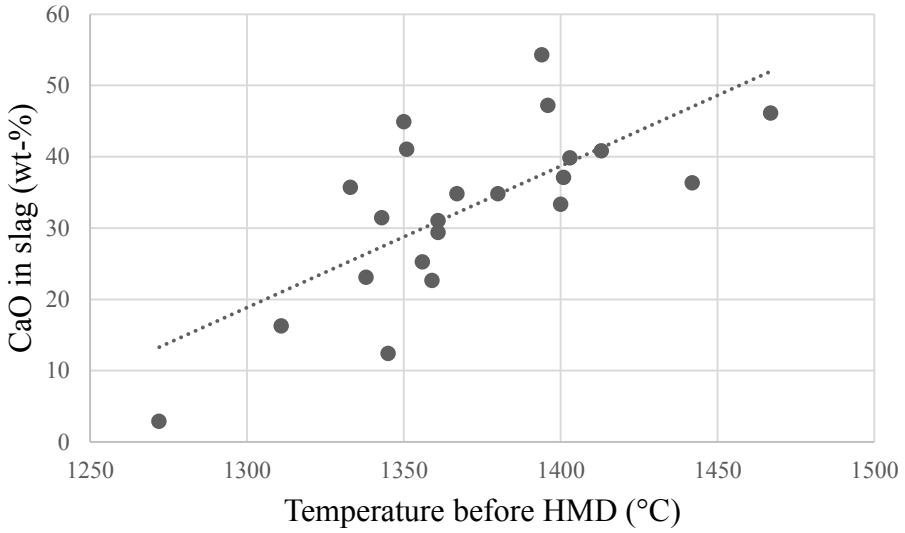

Figure 8. The effect of temperature on the amount of CaO in the slag, where HMD refers to hot metal desulphurisation.

The effect of temperature on the amount of Na_2O in the slag is presented in Figure 9. It appears that the amount of Na_2O in the slag is lower at higher temperatures, which can be attributed to the evaporation of Na and is in agreement with the findings of Li et al. (2015). In one sample, the amount of Na_2O was considerably higher after removing Fe and normalising the composition to 100%. In this sample, the amount of Fe was high, 84 wt-%, which exceeded compositional area that has a reliable analysis tolerance. The amount of CaO in the sample was only 2.89 wt-% after normalisation, which is also visible in Figure 8.

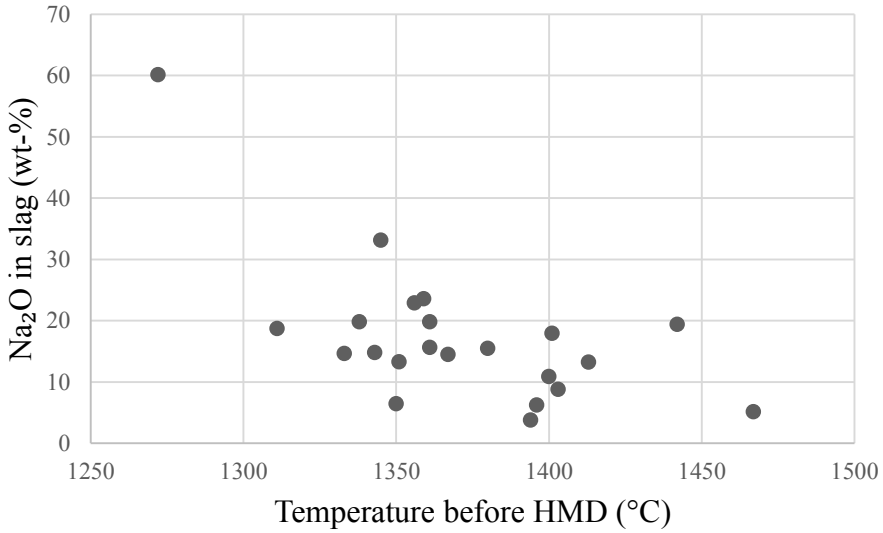

Figure 9. The effect of temperature on the amount of Na_2O in the slag.

7.1.1 Amount of Fe entrapped within the slag

The amount of Fe entrapped within the slag during the campaign was higher than expected. A possible reason for this is that Na_2CO_3 had not been added at the blast furnaces. Unfortunately, the amount of Na_2CO_3 addition was available only for four ladles that were sampled. This data clearly shows that the amount of Fe increases when no Na_2CO_3 is added, which is illustrated in Figure 10. This result is in agreement with the findings of Vuolio (2017).

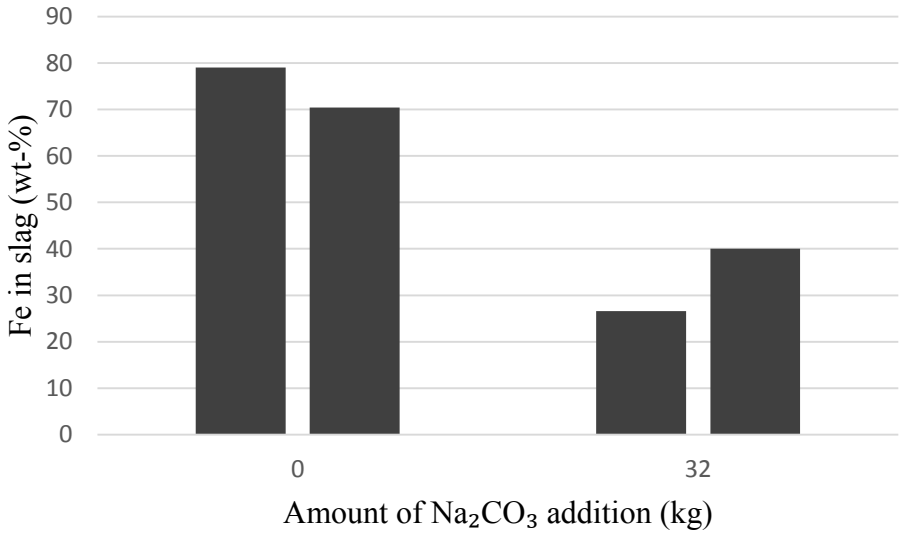

Figure 10. The amount of Fe in slag (wt-%) with Na_2CO_3 additions of 0 and 32 kg.

7.2 Desulphurisation efficiency, sulphide capacity and sulphur distribution ratio of slag

Sulphide capacities of the slags, sulphur distribution ratios and desulphurisation efficiencies of the treatments were calculated using Equation (26), Equation (25), and Equation (13), respectively. The average desulphurisation efficiency, sulphur distribution ratio and sulphide capacity of the dataset are presented in Table 10.

Table 10. The average values of S_{eff}, L_S and $\log(C_S)$ of the dataset.

	S_{eff} (%)	L_S	$\log(C_S)$
Average	79	61	–3.49
Standard deviation	13	35	0.33

The logarithm of the sulphur distribution ratio is plotted against the amount of CaO in the slag in Figure 11. The sulphur distribution ratio seems to increase as a function of the CaO content of the slag. This is in agreement with the findings of Andersson et al. (2000), Zhang et al. (2018), Wu et al. (2018) and Varanasi et al. (2019).

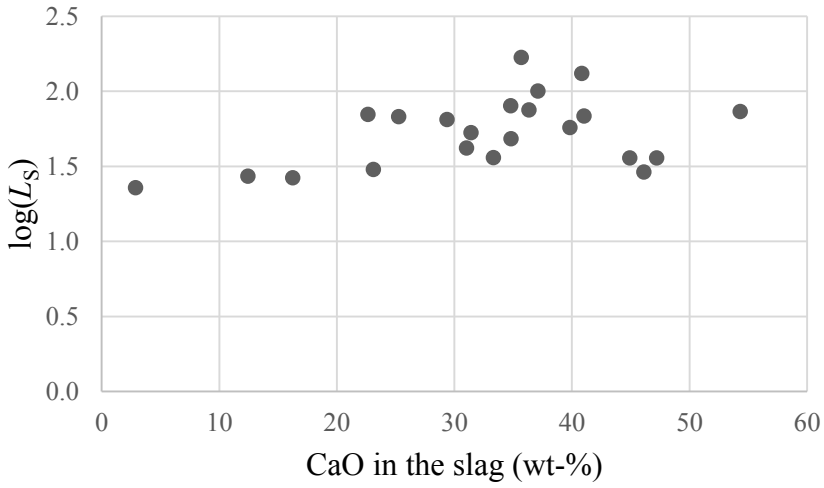

Figure 11. The logarithm of the sulphur distribution ratio as a function of CaO (wt-%) content of the slag.

7.3 Microscopical study

During the sampling campaign, a rapidly cooled piece of initial slag was obtained from sample D1S2 (before) (Day 1 Sample 2, before desulphurisation). The sample was cooled on a metal plate similar to the other samples, and it was chosen for this study based on its appearance. The sample appeared to be molten at the moment of sampling, did not contain excessive amounts of iron, and appeared to have cooled rapidly enough. This glassy piece was then used to make a microsection for microscopical study. The main structures of the sample were studied using light optical microscope images, and the accurate phase compositions were measured by Field Emission Scanning Electron Microscope (FESEM) analyses. It should be noted that the microsection was cut from a larger piece of cooled slag. Thus, it was difficult to identify differences between the middle and the edges of the sample.

Two phases near the edge of the microsection are shown in Figure 12. The dark circles are pores in the sample, and smaller white areas are droplets of Fe.

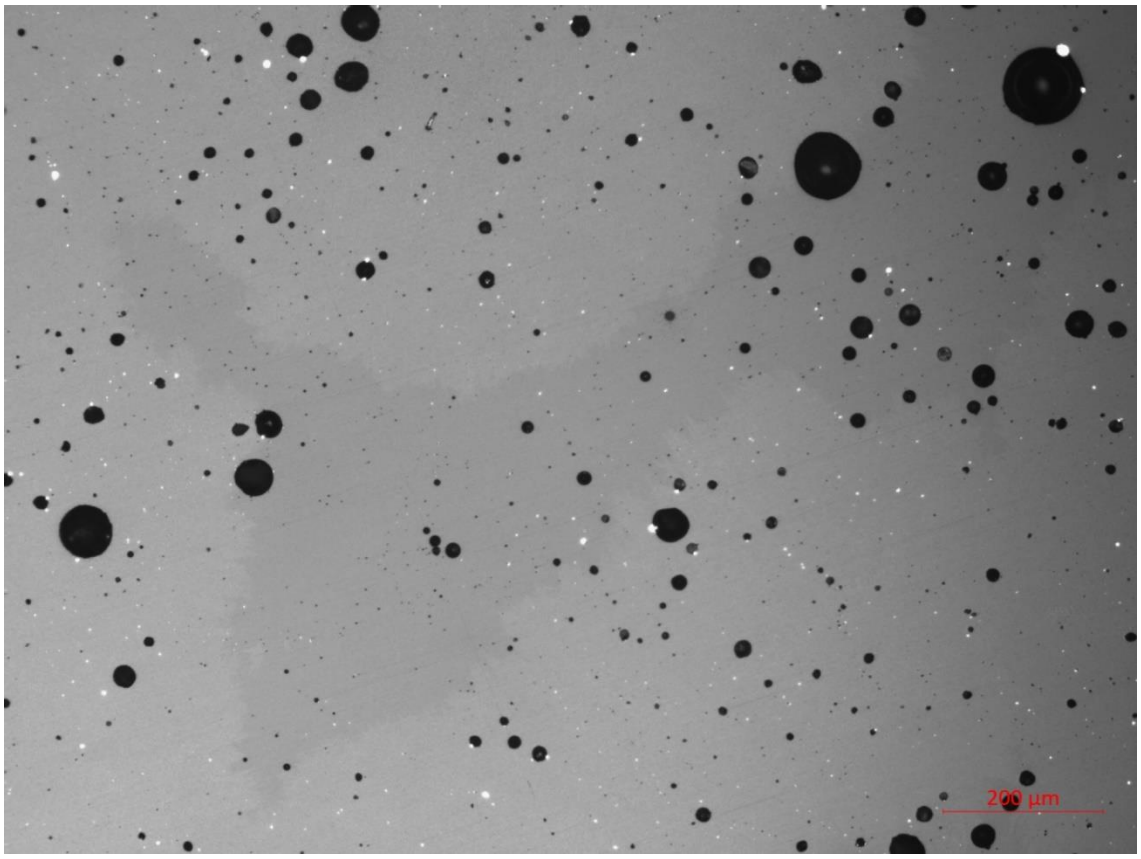

Figure 12. Light optical microscope image near the edge of the microsection.

Dendritic structures were found throughout the sample. The dendrites are a result of the cooling of the sample; a phase has started to crystallise from the glass phase before the sample has solidified. No identification could be made regarding the direction of the dendrites. The dendritic structure is shown in Figure 13.

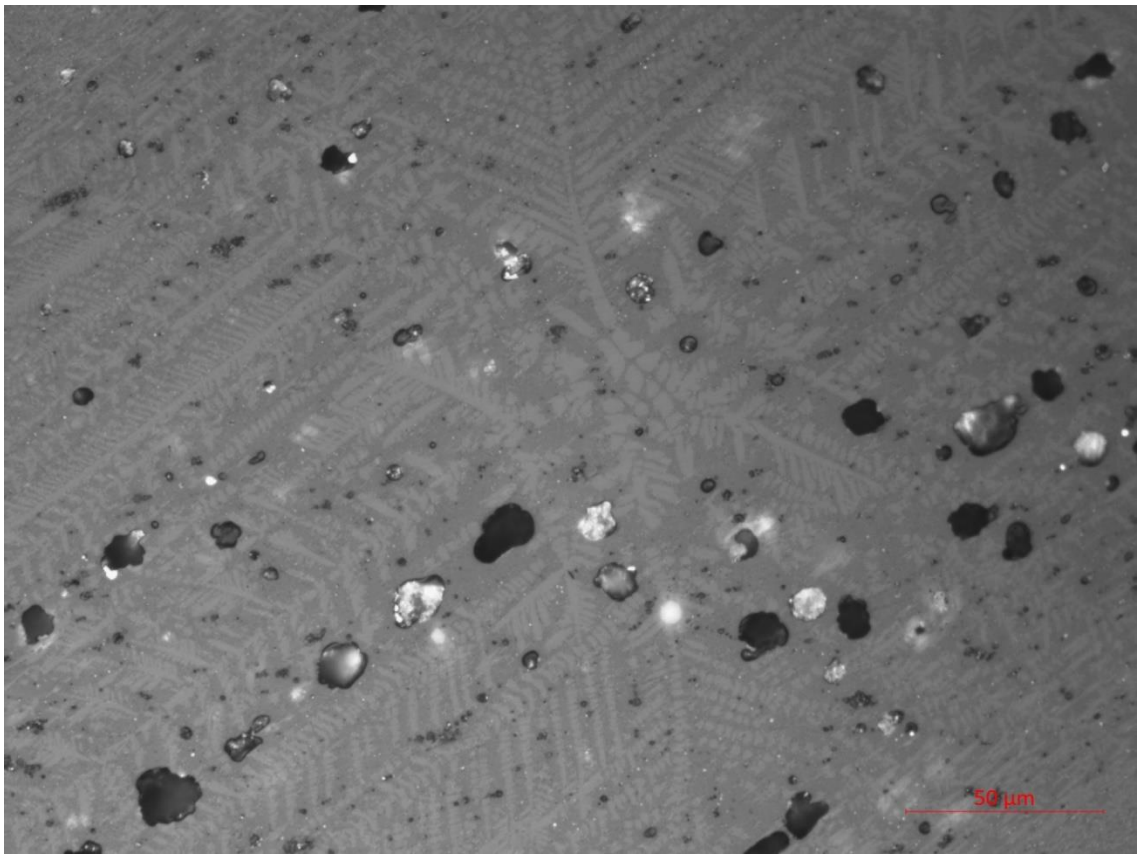

Figure 13. Light optical microscope image of the microsection.

FESEM analyses were carried out at the laboratory of SSAB Europe Oy, Raahe. A FESEM image of a dendritic structure near the edge of the sample and the corresponding analyses of the spectrums are shown in Figure 14 and Tables 11 and 12, respectively. The main phase appears to be a glassy phase from which a larnite phase (dicalcium silicate, Ca_2SiO_4) has started to crystallise before the sample has solidified. This observation indicates that the sample was fully liquid before cooling. Liquid slags are favourable for desulphurisation (Holappa 1980, p. 262; Chiang 1986, p. 90; Kitamura 2014, p. 187–188), and it may be stated that the current initial slag modifying agent has induced the desired effect on the initial slag in this treatment. However, Chiang (1986) has reported that liquid slag is only favourable when the sulphide capacity of the slag is high. With a low sulphide capacity, the slag could cause severe resulphurisation after the slag has reached its refining limit. The composition of the glassy phase was identified to be close to that of melilite ($(Ca,Na)_2(Al,Mg,Fe^{2+})(Si,Al)_2O_7$). However, the sample was cooled so rapidly that no melilite was crystallised in the sample. It was assumed that if the sample had been

cooled slower, a melilite phase and possibly some other phases would have also started to crystallise from the main phase.

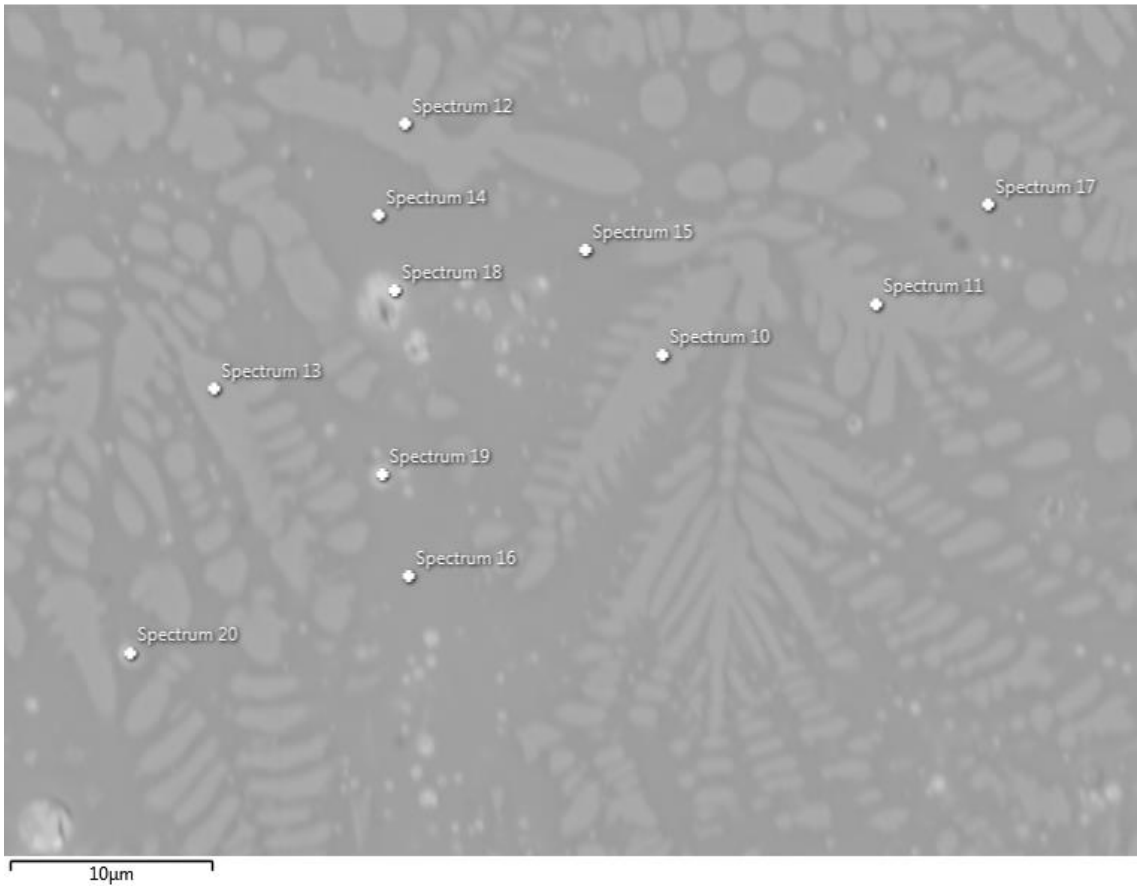

Figure 14. FESEM image of dendritic structure near the edge of the sample.

Table 11. FESEM analyses of the spectrums representing dendritic structure in Figure 16 in oxide-%.

Spectrum	Na_2O	MgO	Al_2O_3	SiO_2	CaO	TiO_2	V_2O_5	Total
10	0.82	0.26	1.58	32.42	56.69	0.64	0.59	93
11	0.54		0.52	32.18	60			93.23
12	0.34			32.2	61.03			93.57
13	0.57		0.96	32.36	59.33			93.22
Average	0.57	0.26	1.02	32.29	59.26	0.64	0.59	93.26

Table 12. FESEM analyses of the spectrums representing the glassy phase in Figure 16 in oxide-%.

Spectrum	Na_2O	MgO	Al_2O_3	SiO_2	S	CaO	TiO_2	V_2O_5	MnO	FeO	Total
14	5.8	1.9	10.47	35.61	1.55	30.91	4.6	0.49	0.73	1.79	93.86
15	5.84	1.82	10.97	35.6	1.27	30.31	4.74	0.69	1.07	1.62	93.93
16	5.32	2.05	9.24	36.16	1.95	31.97	4.52		0.95	1.63	93.78
17	5.76	2.02	10.74	35.83	1.58	30.29	4.98		1.14	1.64	93.98
Average	5.68	1.95	10.36	35.80	1.59	30.87	4.71	0.59	0.97	1.67	93.89

8 RESULTS OF THE INDUSTRIAL TEST-RUN

During the industrial test-run, a total of 15 ladles were sampled, of which two initial slag samples failed. Thus, the complete data available for analysis contains 13 experiments, of which 7 represent LS addition and 6 represent LS and Na_2CO_3 addition. The average temperature and composition of the initial slag in both cases are presented in Table 13. The initial slag was observed to be molten during sampling throughout the test-run, even without the addition of Na_2CO_3.

Table 13. The average temperature and composition of initial slag during the test-run.

	T_0	K_2O	Na_2O	S	MgO	Al_2O_3	SiO_2	CaO	Fe	B
LS	1403	0.09	5.00	1.32	1.94	9.14	33.41	34.01	11.77	1.02
St. dev.	24	0.02	5.64	0.72	0.33	2.03	3.28	6.81	8.02	0.20
LS + Na_2CO_3	1401	0.08	12.58	2.40	2.23	8.78	33.42	33.32	7.11	1.00
St. dev.	20	0.03	3.21	0.82	0.51	1.54	1.76	1.62	4.33	0.08

The desulphurisation slag was also sampled during the test-run, and the composition is presented in Table 14. The data contains also the experiments during which the initial slag samples failed. By interpreting the analyses of the desulphurisation slag, it appears that the slag is solid due to high amounts of CaO originating mainly from the injected reagent.

Table 14. The composition of the desulphurisation slag during the test-run.

	K_2O	Na_2O	S	MgO	Al_2O_3	SiO_2	CaO	Fe	B
LS	0.04	2.20	2.48	0.62	1.46	7.63	35.70	43.96	4.99
St. dev.	0.01	0.61	1.01	0.17	0.84	2.71	7.73	12.69	0.93
LS + Na_2CO_3	0.05	3.15	1.86	0.72	1.42	7.41	38.33	38.78	6.62
St. dev.	0.02	0.48	0.80	0.22	0.71	3.30	8.05	12.71	4.05

8.1 Composition

The predicted compositions of initial slag calculated prior to the industrial test-run were compared to the measured compositions during the test-run. Slag components not included in the predicted compositions were removed from the measured compositions, and the compositions were then normalised to 100 wt-%.

It was discovered that the amount of Fe entrapment was higher in the predicted compositions than during the test-run, especially in the case of no Na_2CO_3 addition. Thus, the study was also carried out for Fe-removed and normalised slag compositions. Lower Fe entrapment coupled with the observations of liquid slag throughout the test-run indicate that LS had succeeded in fluidising the slag.

8.1.1 LS addition

The predicted compositions and the average composition of initial slag in the case of LS addition are presented in Figure 15 in the form of a stacked bar chart. It can be seen from the figure that the amount of Fe entrapment is two to four times larger in the predicted compositions. Due to large differences in the Fe content of the slag, it is difficult to estimate the accuracy of the other predicted components. However, with respect to SiO_2 and Al_2O_3, it appears that the average of the measured compositions corresponds better to the predictions with a large mass of initial slag.

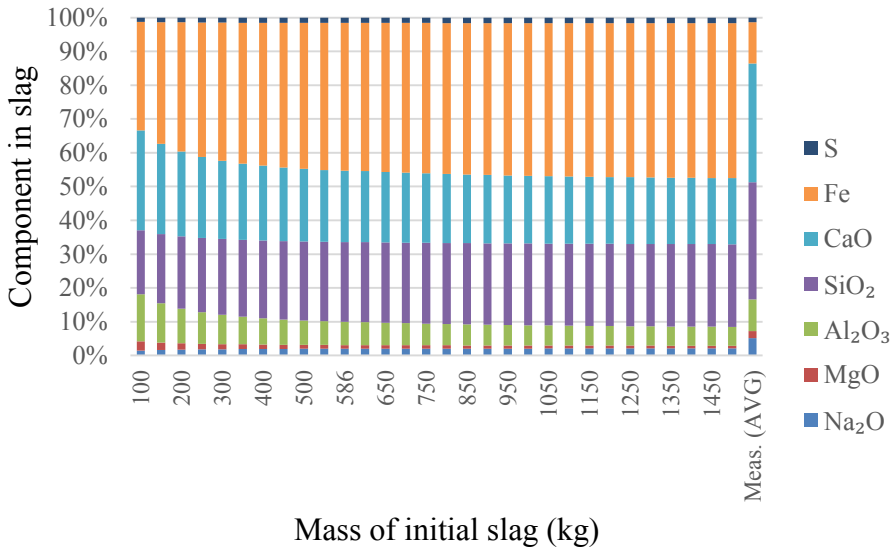

Figure 15. The predicted compositions of initial slag combined with the average of the measured compositions in wt-% in the case of LS addition.

After removing Fe and normalising the compositions, diagrams similar to Figure 15 were utilised to detect similar slag compositions. In Figure 16, the predicted composition when the mass of the initial slag is 200 kg is presented along with the

average of the measured compositions. After removing Fe, the predicted composition appears to correspond better to the measured slag composition, although Na_2O, Al_2O_3 and CaO differ by a few wt-%. A possible explanation for this is variation in the origin of initial slag: a higher CaO content indicates that the amount of CaO-bearing skull in initial slag is higher. The difference in the Na_2O content may be attributed to two samples, in which the Na_2O content was substantially higher. The sulphur distribution ratio seems to be lower than expected, which is visible in the lower sulphur content of the slag phase when compared to the predicted value.

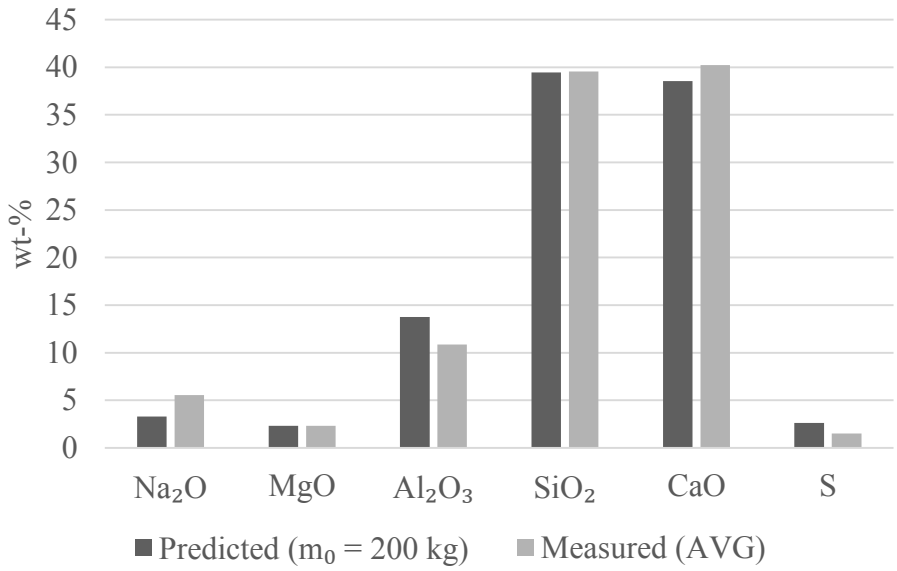

Figure 16. The predicted composition if initial slag (m_0 = 200 kg) and the average of the measured compositions in the case of LS addition.

8.1.2 LS & Na_2CO_3 addition

The predicted compositions and the average composition of initial slag in the case of LS and Na_2CO_3 addition are presented in Figure 17 in the form of a stacked bar chart. It can be deduced from the figure that in the case of both LS and Na_2CO_3 addition, the predicted slag compositions correspond better to the measured compositions than in the case of LS addition. The amount of Fe entrapped in the slag is still higher in the predicted compositions, but the difference is not as significant. The relatively high fraction of Al_2O_3 in the average of the measured slag compositions implies that the composition correlates better to predictions with low masses of initial slag.

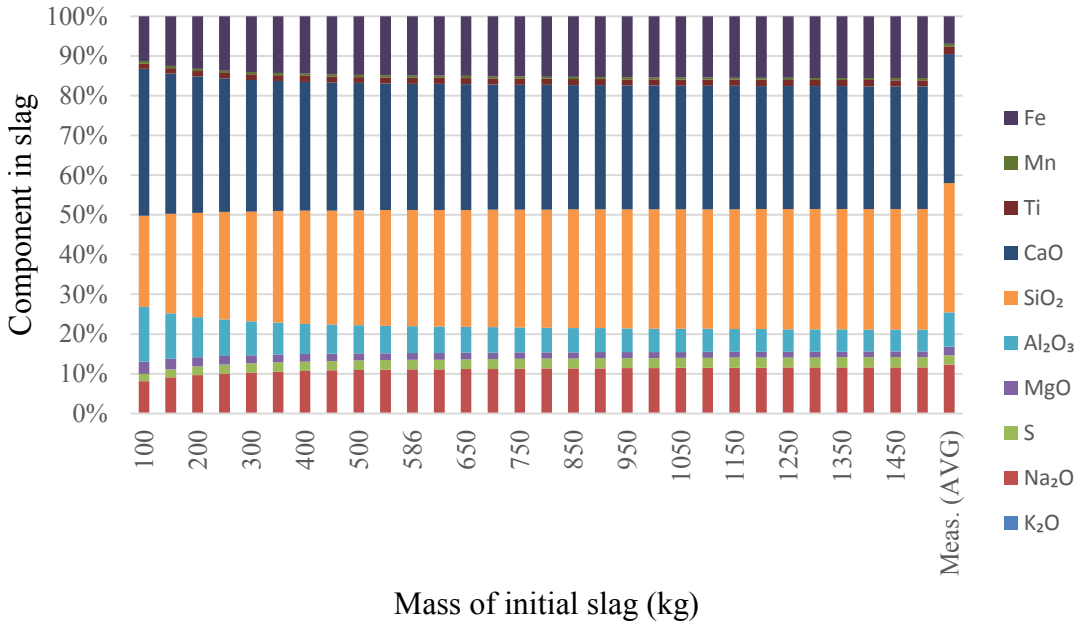

Figure 17. The predicted compositions of initial slag combined with the average of the measured compositions in wt-% in the case of LS and Na_2CO_3 addition.

In Figure 18, the average of the measured compositions after removing Fe is presented with the predicted composition when the mass of the initial slag is 586 kg. It can be seen from the figure that with respect to Na_2O and SiO_2, the compositions correspond well to each other. Only CaO and Al_2O_3 exhibit a difference of a few percentage points.

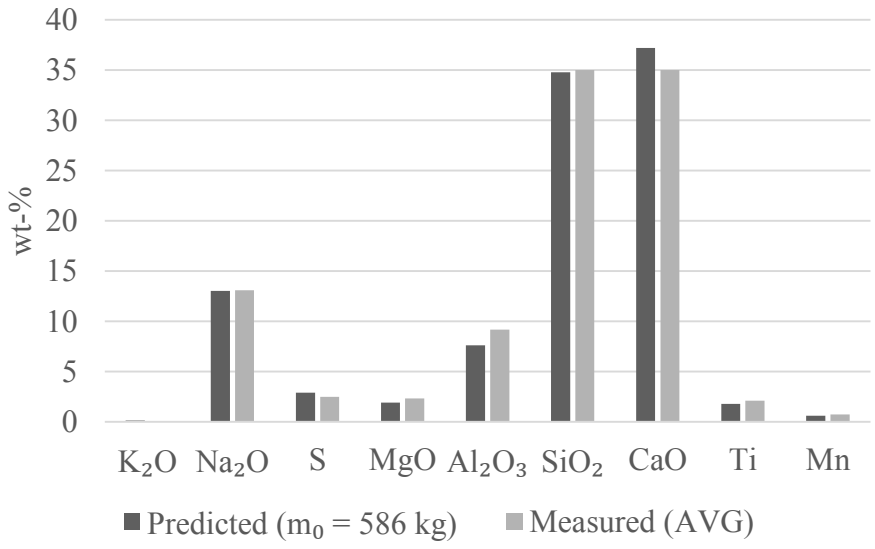

Figure 18. The predicted composition (m_0 = 586 kg) and the average of the measured compositions during the test-run in the case of LS and Na_2CO_3 addition.

8.2 Mass of the initial slag

The approximated mass of the initial slag obtained for the case of LS addition was 185.4 kg. In Figure 19, the predicted composition with this amount of initial slag is presented along with the average of the normalised measured compositions during the test-run. The difference in the Na_2O content may be attributed to two samples in which the weight percentage of Na_2O was substantially higher. This may be a result of Na_2CO_3 addition at the BF, although it was instructed otherwise. The higher Al_2O_3 content in the predicted composition indicates that the mass of the initial slag was in fact higher during the test-run. When the mass of the initial slag is higher, the effect of Al_2O_3-bearing LS on initial slag is lower. On the other hand, differences in the Al_2O_3 content may also be due to different rates of refractory wear, which were not addressed in the study. If this would be the case, then it would seem that the use of LS decreases refractory wear. The difference in the compositions may be also attributed to differences in the amounts of two main components, SiO_2 and CaO, between the slag samples used for the predicted compositions and those collected during the test-run.

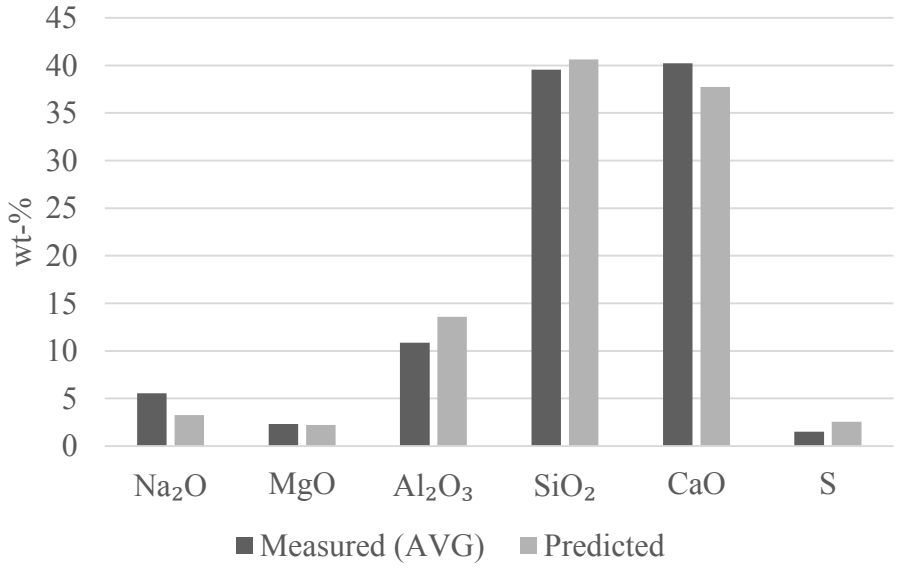

Figure 19. The average of the normalised measured compositions of the initial slag in the case of LS addition, combined with the predicted composition (m_0 = 185.4 kg).

For the case of LS & Na_2CO_3 addition, the obtained approximation for the mass of the initial slag was 372.3 kg. The predicted composition with this amount of initial slag is

presented along with the average of the normalised measured compositions during the test-run in Figure 20. The predicted CaO content appears to be a few wt-% units higher than in the measured slag, whereas the weight percentages of Na_2O, SiO_2 and Al_2O_3 are lower. This is most likely due to differences in the constituents of initial slag: a lower CaO content in the measured composition indicates that the amount of skull in the initial slag is lower, meanwhile Na_2O and SiO_2 originating mainly from Na_2CO_3 and BF slag, respectively, are higher.

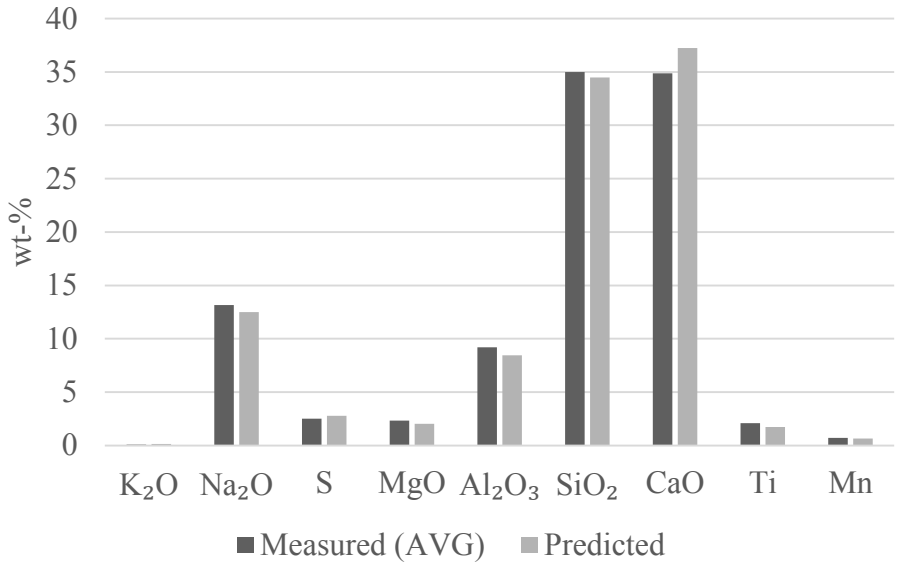

Figure 20. The average of the normalised measured compositions of the initial slag in the case of LS & Na_2CO_3 addition, combined with the predicted composition (m_0 = 372.3 kg).

8.3 Origin of the slag components

The origin of the slag components was studied, and the results can be seen in Table 15. The samples are named so that Series 1 (S1) refers to LS addition, and Series 2 (S2) refers to LS & Na_2CO_3 addition. For two experiments in Series 1, the value of SSE was significantly higher than the corresponding value for other treatments. This was mostly due to high amounts of Na_2O in the samples. In two experiments in Series 2, the amount of Si in hot metal samples increased between the BF and the desulphurisation plant, which caused error in the predicted compositions. This can be seen in the results of

sample S2E8 (before). The amount of SiO_2 removed from the slag is so large that the amounts of BF slag and skull converge to their maximum value, which was constrained to 1000 kg. If the maximum limits for BF slag and skull were not constrained, the solution converged to SSE = 249.4, which corresponds to $m_{BF\ slag}$ = 64505 kg and m_{skull} = 15495 kg. This may be partly due to the fact that the BF slag is sampled from the slag runner. The composition of the BF slag in the hot metal ladle may thus differ from the composition of the analysed slag, which leads to poor applicability of BF slag in the calculations. However, there might also be a high uncertainty in the measured composition of the slag from the ladle.

Table 15. The predicted origin and total mass of initial slag during the test-run.

Sample	m_{tot} (kg)	$m_{BF\ slag}$ (wt-%)	m_{skull} (wt-%)	$m_{SiO_2\ (ox.)}$ (wt-%)	SSE
S1E1 (before)	380.0	12.3	52.3	22.3	8.58
S1E2 (before)	630.1	41.2	35.3	15.5	267.00
S1E3 (before)	512.3	0	74.5	15.7	33.19
S1E4 (before)	466.2	31.3	32.2	25.7	275.24
S1E5 (before)	495.5	0	73.7	16.2	17.11
S1E6 (before)	773.5	29.1	45.8	18.6	15.63
S1E7 (before)	158.0	0	43.1	25.3	22.56
S2E1 (before)	431.3	5.6	55.9	22.6	49.24
S2E2 (before)	360.8	81.0	0	–5.3	319.10
S2E3 (before)	178.7	0	41.8	19.8	24.14
S2E4 (before)	221.5	0	42.8	26.2	20.47
S2E7 (before)	236.5	23.3	35.9	11.8	66.97
S2E8 (before)	1403.3	71.3	71.3	–47.4	2751.46
Average	480.6	22.7	46.5	12.8	297.74

Comparison between the measured and predicted compositions of initial slag in sample S1E1 (before) is provided in Figure 21. The compositions correspond reasonably well to each other, indicating that the mass of the initial slag could in fact have been higher than estimated by using the predicted compositions that were calculated prior to the test-run. The amount of MgO was fairly accurately predicted. MgO originates only from BF slag and LS, thus indicating that the amount of BF slag in this experiment (46.6 kg) can be stated to have been predicted with reasonable accuracy. With respect to MgO, there is a maximum value that the amount of BF slag could theoretically reach. Considering that

BF slag contains around 10 wt-% of both MgO and Al_2O_3, large amounts of BF slag should also lead to higher MgO contents of the initial slag. However, the amount of MgO in initial slag varies around 2–3 wt-%, implying that the predicted amount of BF slag in some experiments was higher than theoretically possible. This may be partly attributed to an increase in the Si content of the hot metal samples, indicating the reduction of SiO_2 from slag to the hot metal. This leads to the amount of SiO_2-bearing BF slag reaching higher values in the calculations.

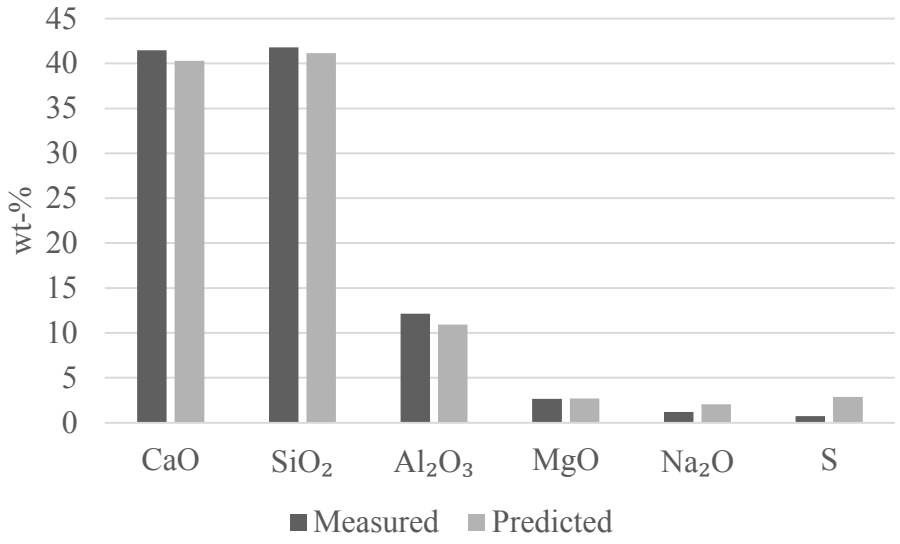

Figure 21. The measured and the predicted composition of sample S1E1 (before) (SSE = 8.58).

The amount of BF slag corresponding to the number of ladles during tapping is presented in Figure 22. There were four experiments in which the obtained amount for BF slag was 0 kg. Two of these were the first, one was the third and one was the fourth ladle of the tapping. The amount of BF slag seems to be lower in the ladles that were filled first during the tapping. A logical reason for this may be that during the filling of the first ladle, slag had not started to exit the BF yet.

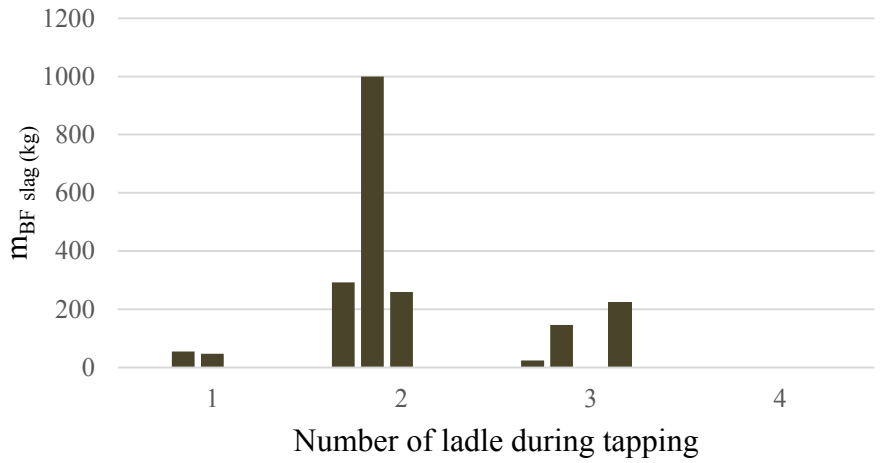

Figure 22. The amount of BF slag corresponding to the number of ladles during tapping.

8.4 Sulphide capacity and sulphur distribution ratio of slag

Sulphide capacities of the slags were calculated using Equation (26) and the sulphur distribution ratios of the treatments were calculated using Equation (25). The results are presented in Table 16. Sulphide capacities and sulphur distribution ratios of the slags were higher when both LS and Na_2CO_3 were added to the ladle, as was expected based on the predicted sulphide capacities of the slags prior to the test-run. It follows from Equation (26) that the sulphide capacity increases with an increase in the sulphur distribution ratio of the slag.

Table 16. The sulphide capacities and sulphur distribution ratios of the slags during the test-run.

	T_0 (°C)	$\log(C_S)$	L_S
Average (LS)	1403	–3.76	21
Standard deviation	24	0.19	9
Average (LS & Na_2CO_3)	1401	–3.39	52
Standard deviation	20	0.18	23

The sulphide capacities of the slags were also calculated utilising the model proposed by Young et al. (1992) for comparison. This was done for the complete dataset, including the sampling campaign, the samples collected previously by Vuolio (2017),

the test-run, and the samples that were excluded from other studies. The slag samples collected during this work are presented in Appendix 1. For two samples from the sampling campaign, the model suggested a negative value for the slag's sulphide capacity. This was attributed to the optical basicity of the slag being over 0.8; this led to using Equation (31) for calculating the sulphide capacity. Equation (31) makes use of the wt-% FeO parameter, and FeO was not included in the XRF analysis method utilised for obtaining the chemical composition of the slag. It was assumed that Fe in the sample occurred mainly as metal droplets, thus the amount of FeO in the sample was estimated based on FESEM analysis of a different sample. Assuming that the amount of FeO in the samples is equal is obviously a major uncertainty in the calculations. However, it was also assumed that the model does not perform well when the optical basicity of the slag is over 0.8.

Comparison between the measured and predicted sulphide capacities of the slags is shown in Figure 23. The measured sulphide capacities refer to those calculated using Equation (26). It can be seen from the figure that there is deviation in both directions in the values predicted using the model. The poor correlation of the predicted and measured values is most likely due to the poor accuracy of the model proposed by Young et al. (1992). The model makes use of the optical basicity concept, temperature, and weight percentages of a few slag components, whereas Equation (26) considers the activity of oxygen and activity coefficient of sulphur in metal, as well as the sulphur distribution ratio and the equilibrium constant of Equation (23).

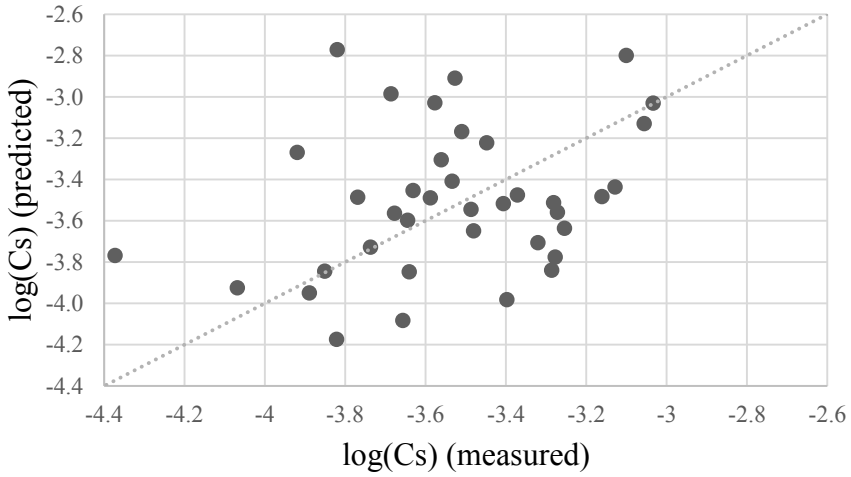

Figure 23. Comparison between the measured sulphide capacities and those calculated utilising the model proposed by Young et al. (1992).

8.5 Analyses of the hot metal samples

Analyses made utilising the analyses of hot metal samples are discussed in this section. The analyses of hot metal samples are presented in Appendix 2. The analyses do not exhibit significant variance and hence are not presented here separately.

8.5.1 Desulphurisation efficiency

Desulphurisation efficiencies of the treatments were calculated using Equation (13). The average desulphurisation efficiency during the test-run was 92%, which is 13% higher than during the sampling campaign. The highest value was 97% and the lowest 84%. However, samples were not collected from treatments without LS addition during the test-run. Therefore, it cannot be stated that the higher desulphurisation efficiencies would necessarily be due to the use of LS in initial slag modification. An interesting observation was that the average desulphurisation efficiency did not vary between the two different test series. One explaining factor for this may be that the average consumption of the desulphurisation reagent during Series 1 was higher by 0.05 kg/tHM.

8.5.2 Comparison between hot metal samples taken at the blast furnace and at the desulphurisation plant

The hot metal samples collected during the test-run were compared to those taken at the BF. The averages of the analyses are presented in Table 17. All components were analysed utilising the X-ray fluorescence (XRF) method, because the needs of the process do not allow the analysis of C and S by the combustion method, which is more time consuming. In Figure 24, comparison between the sulphur contents of hot metal in the samples is presented. The figure shows that there is notable sulphur reversion (50–100 ppm) to hot metal in three of the ladles sampled, thus implying that in these cases the sulphur distribution ratio during the transport of hot metal has been higher than at slag-metal equilibrium, as described by Vuolio et al. (2019). In one experiment, the sulphur content of the hot metal decreased by 72 ppm during the transport, indicating the occurrence of desulphurisation through the permanent contact reaction.

Table 17. The averages of the analyses of the hot metal samples taken at the blast furnace and the desulphurisation plant during the test-run (wt-%).

Average	C	S	Si	P	Ti	V	Cr	Mn	Ni	Cu
BF	4.57	0.0504	0.450	0.056	0,075	0.284	0.043	0.232	0.030	0.009
HMD (before)	4.64	0.0519	0.436	0.054	0,074	0.285	0.044	0.232	0.033	0.009

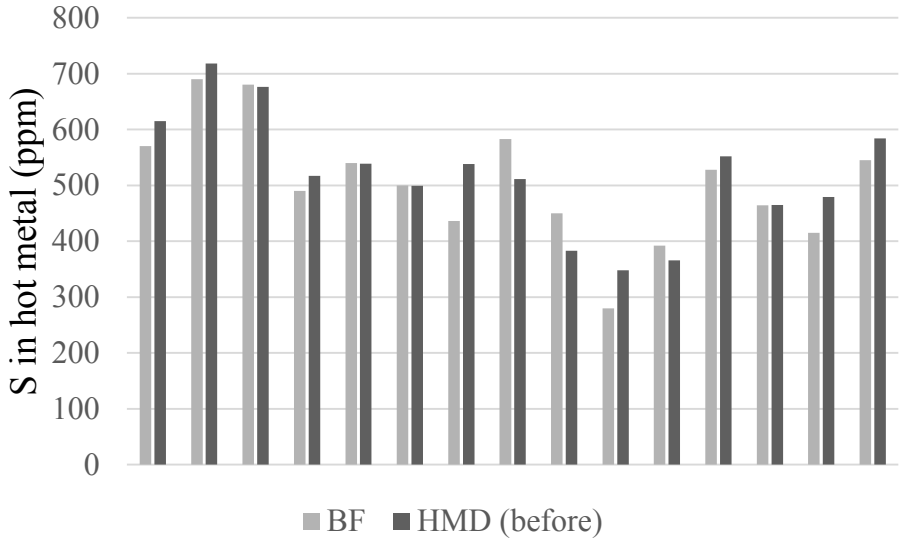

Figure 24. Comparison between the sulphur contents of the hot metal samples taken at the blast furnace and at the desulphurisation plant.

8.6 Effect of slag composition on the desulphurisation process

A model for predicting the sulphide capacity of the slag phase was identified. The explanatory variables of the model and corresponding information are presented in Table 18. It can be deduced by interpreting the regression coefficients that Na_2O and CaO in the slag as well as the temperature increase the sulphide capacity, whereas the presence of Mn in the slag decreases it. The *t*-test shows that the regression coefficient estimates are reliable, and thus the explanatory variables in the subset can be stated to have a statistically significant effect on the sulphide capacity. By interpreting the VIF-values of the explanatory variables, it can be concluded that there is no collinearity problem related to them.

Table 18. The explanatory variables of the prediction model for the sulphide capacity of the slag.

	Unit	Coefficient	SE	*t*-value	P-value	VIF
Intercept	–	–6.74726	0.8820	–7.65	$5.65 \cdot 10^{-9}$	–
(Na_2O)	wt-%	0.033229	0.0042	7.93	$2.51 \cdot 10^{-9}$	1.37
(CaO)	wt-%	0.011622	0.0024	4.81	$2.85 \cdot 10^{-5}$	1.65
(Mn)	wt-%	–0.16779	0.0375	–4.47	$7.86 \cdot 10^{-5}$	1.22
T_0	°C	0.001905	0.0006	2.99	$5.1 \cdot 10^{-3}$	1.79

The predicted sulphide capacities are plotted as a function of the measured sulphide capacities in Figure 25. As can be seen from the figure, the present model performs better with the present dataset than the model proposed by Young et al. (1992). $R^2_{\text{adj.}}$ for the model is 0.77, which means that 77 % of the variation in the sulphide capacity can be explained by the applied explanatory variables and is therefore an indication of a decent fit. MAE of the model is 0.11.

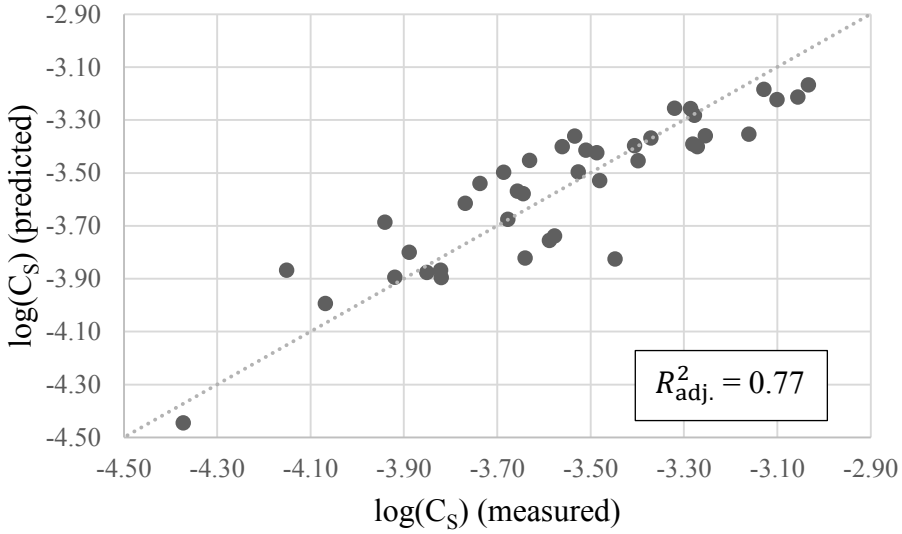

Figure 25. Comparison between the measured and predicted sulphide capacities.

In Table 19, the explanatory variables and corresponding information related to the developed prediction model for desulphurisation efficiency are presented. As can be seen from the table, all explanatory variables have an increasing effect on desulphurisation efficiency, which is not ideal for a model. In addition, desulphurisation efficiency increased with increasing Al_2O_3 content of the slag, whereas in the literature some studies suggest the opposite effect of Al_2O_3 in the slag on desulphurisation (Choi et al. 2001; Varanasi et al. 2019). The predicted desulphurisation efficiency is plotted as a function of the measured desulphurisation efficiency in Figure 26. It can be deduced from the figure that the model suffers from the LOF phenomenon, i.e. the model does not elucidate well the variation in desulphurisation efficiency. This usually implies that some important explanatory variables are missing from the model. The residuals of the model were plotted against the explanatory variables, and no correlations were found. By interpreting the VIF values, multicollinearity can be ruled out. $R^2_{\text{adj.}}$ and MAE for the model are 0.61 and 5.42%, respectively.

Table 19. The explanatory variables of the prediction model for desulphurisation efficiency.

	Unit	Coefficient	SE	*t*-value	P-value	VIF
Intercept	%	–55.9077	33.78	–1.65	0.11	–
$m_{reag.}$	kg/tHM	2.811557	0.63	4.50	$7.23 \cdot 10^{-5}$	1.70
[C]	wt-%	19.53208	6.78	2.88	$6.7 \cdot 10^{-3}$	2.40
$a^{H}_{[S]}$	–	72.85621	27.22	2.68	0.01	2.50
(Al_2O_3)	wt-%	1.002505	0.42	2.37	0.02	1.26

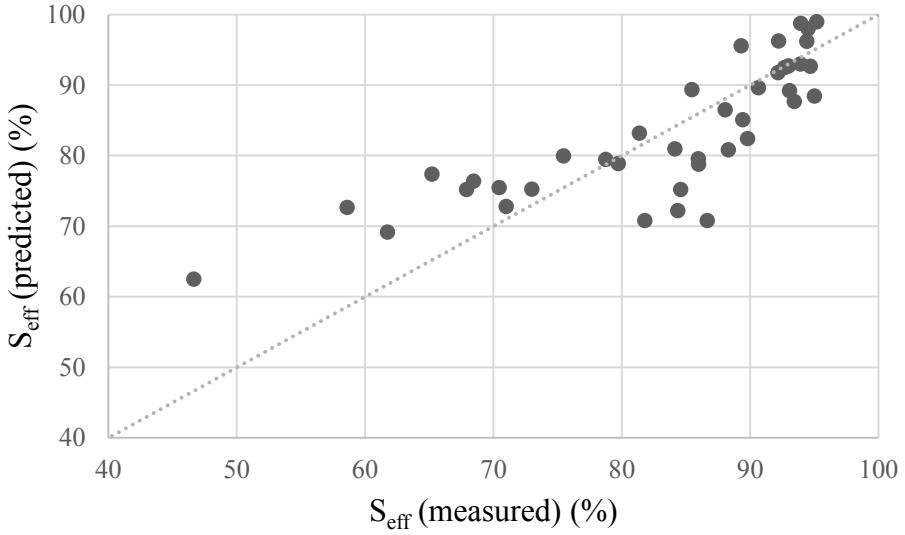

Figure 26. Comparison between the measured and predicted desulphurisation efficiencies.

The explanatory variables and corresponding information regarding the model that was developed for predicting the sulphur content of the hot metal after desulphurisation are presented in Table 20. Slag properties did not perform well as explanatory variables in the model and were thus not included. The amount of sulphur in hot metal before desulphurisation exhibited correlation with the response variable with some groups of variables, but due to low values of $R^2_{\text{adj.}}$ it was not included in the final model. According to the model, the logarithm of the Henrian equilibrium activity of oxygen in hot metal decreases the value of the response value. However, low oxygen activity in hot metal is favourable for desulphurisation (Kitamura 2014, p. 180). Thus, the sign of the regression coefficient of the explanatory variable is wrong. A possible explanation for this is that the initial sulphur content of hot metal was excluded from the model

while C in hot metal was included. Comparison between the measured and predicted sulphur contents of hot metal after desulphurisation is presented in Figure 27. $R^2_{\text{adj.}}$ and MAE for the model are 0.68 and 24 ppm, respectively.

Table 20. The explanatory variables of the prediction model for sulphur content of the hot metal after desulphurisation.

	Unit	Coefficient	SE	*t*-value	P-value	VIF
Intercept	ppm	553.5169	189.8307	2.92	$6.07 \cdot 10^{-3}$	–
$m_{reag.}$	kg/tHM	−13.6756	2.352804	–5.81	$1.24 \cdot 10^{-6}$	1.31
[C]	wt-%	−154.462	22.8941	–6.75	$7.07 \cdot 10^{-8}$	1.48
$\log a^{H}_{[O]}$	–	−100.804	30.52755	–3.30	$2.17 \cdot 10^{-3}$	1.15

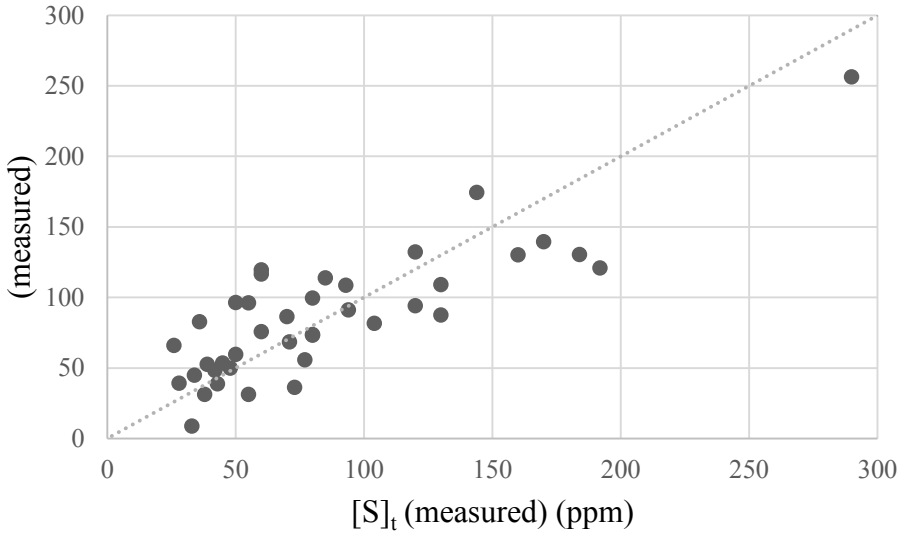

Figure 27. Comparison between the measured and predicted sulphur contents of hot metal after desulphurisation.

The two latter prediction models were less successful in explaining the variation in the response variable than the sulphide capacity model. $R^2_{\text{adj.}}$ values were 0.61 and 0.68 for the S_{eff} model and the S_t model, respectively. It can be seen in Figure 26 that the prediction model for desulphurisation efficiency yields too high values when the response variable is low. In the case of the S_t model in Figure 27, the predicted values are more evenly distributed around the line that represents perfect fit. However, the standard error of the model is relatively large. In addition, the models only contained

explanatory variables which had regression coefficients of the same sign. All of the variables in the S_{eff} model increased the value of the response variable, and in the S_t model all of the variables decreased it. The VIF values of the explanatory variables indicate that there are no collinearity problems in either of the two models.

The aim of the regression modelling was to study the applicability of slag properties as explanatory variables in the models. The sulphide capacity of slag, as described in Section 5.3, depends only on the slag properties and the temperature. Thus, the weight percentages of the selected slag components and the temperature before desulphurisation proved to be statistically relevant in predicting the value of the response variable in terms of the applied *t*-test. In the prediction model for desulphurisation efficiency, the amount of Al_2O_3 in the slag phase exhibited statistical significance in terms of the applied *t*-test, but the sign of the regression coefficient was wrong. Thus, the competence of the model is debatable. In the case of the prediction model for sulphur content of hot metal after desulphurisation, no slag properties proved statistical significance in the model. Therefore, the effect of slag properties on the desulphurisation process could not be further elucidated by the applied MVLR modelling based on this dataset.

9 PROPOSITIONS FOR FURTHER WORK

This thesis aimed at elucidating the variance in the composition and amount of initial slag in primary desulphurisation of hot metal, as well as discovering the effect of initial slag on the efficiency of the desulphurisation process. In the following, some future actions regarding the study and use of initial slag in hot metal desulphurisation are proposed.

9.1 The effect of initial slag on the desulphurisation of hot metal

The amount of initial slag samples collected during this work was rather small. By combining the data with the samples collected previously by Vuolio (2017), a dataset sufficient in size for subsequent analysis was obtained. However, the effect of initial slag on the desulphurisation process was not further elucidated by the applied MVLR modelling, implying the need for more initial slag samples. This was apparent also from the results of the applied models; according to the model constructed for predicting desulphurisation efficiency, Al_2O_3 in the slag phase had the opposite effect on desulphurisation than it should based on the found literature. With a larger dataset, the effects of individual slag components on desulphurisation of hot metal could possibly be more easily discovered. Other methods of analysis could also be useful for application to further studies. For example, the effects of different variables on desulphurisation parameters might not be linear. Thus, nonlinear methods of analysis could yield valuable information.

9.2 The use of ladle slag in initial slag modification

The results obtained and observations made during the industrial test-run were positive with respect to the initial slag. Thus, the use of LS in initial slag modification should be further studied.

In order to further study the use of LS, a more comprehensive test-run should be conducted, during which the following matters should be assessed:

- The use of LS & Na_2CO_3: currently, the use of both LS & Na_2CO_3 seems to be the most attractive option. By conducting a longer test-run, different amounts of both initial slag modifying agents should be tested in order to find the optimum amount of both agents. Also, different amounts of added LS should be tested in order to discover possible non-linear impacts. For example, the estimated liquid fractions indicate that the effect of LS on the liquid fraction of initial slag is not linear.
- Refractory wear was not studied in this work. During the test-run, LS was added before Na_2CO_3 in order to protect the ladle refractories from the wearing effect of Na_2CO_3. During future test-runs, the wearing effect of LS should be studied, and the most feasible addition method should be investigated, i.e. LS before Na_2CO_3, LS-Na_2CO_3-mixture and so on.
- Skulling: during a longer test-run, it would be advantageous to observe the bottoms of empty ladles in order to discover whether the added LS forms skulls. This should be also linked to the method of addition; should skulls be observed, could it be avoided by using a mixture of the two agents instead of adding LS first on the bottom of the ladle?

There are large amounts of LS produced annually, but the economic aspects of the use of LS were not studied in this thesis. Some issues concerning the use of LS still remain, including:

- The annual production rate: Is the amount of LS produced sufficient for the needs of the initial slag modification? The study should be also conducted for a larger addition of LS, should that prove more attractive in the future.
- The profitability of the use of LS: Currently, LS is being sold for other uses. The financial aspects of the use of LS in initial slag modification should be looked into, in addition to whether the savings are larger than the lost income.

9.3 Alternative materials for initial slag modification

In this work, a brief literature review on different initial slag modifying agents was conducted. There were two groups of modifying agents that have been tested with

promising results elsewhere and could be advantageous to study further and test in operation.

Nepheline syenite, or more accurately nepheline syenite tailings, seem an applicable option for initial slag modification. NST contains around 15 wt-% alkalines (Na_2O and K_2O), first of which is widely known to be a favourable slag component with respect to desulphurisation and is presently used to fluidise the slag. NST is a by-product of the glassware industry, and hence should be readily available.

Na_2O-SiO_2-CaF_2-based agents have been successfully tested in industrial operation in China. The results were very positive with respect to slag skimming times, desulphurisation efficiency and heat losses during powder injection. (Diao et al. 2009) Bearing in mind these results, an initial slag modifying agent of a similar composition could be beneficial to develop and test in operation. The amount of SiO_2 should be kept low, since as an acidic compound it decreases the basicity of the slag and thus is detrimental for desulphurisation in high amounts. Only the minimum about of CaF_2 should be used to achieve the fluidising effect in the initial slag, while also minimising the harmful effects of CaF_2.

9.4 The contribution of blast furnace slag to the composition of initial slag by mass balance equations based on MgO

Earlier in this thesis, it was stated that MgO in initial slag originates only from BF slag and LS, if added. Thus, the contribution of BF slag to the composition of initial slag could theoretically be solved by utilising mass balance equations with respect to MgO. If the amount of initial slag is known, i.e. if the measurement of the thickness of the slag layer succeeds in the future, the amount of BF slag in initial slag could be accurately calculated. The calculations would also be possible based on the dataset of the present test-run. This is an aspect worth inspecting in the future, since the estimations for the amount of BF slag reached high values in some of the present calculations, mostly due to the [Si]-(SiO_2) equilibrium.

10 CONCLUSIONS

The aims of this thesis were three-fold:

- to estimate the composition and amount of initial slag as well as their variances in primary desulphurisation of hot metal,
- to discover the effect of initial slag on the efficiency of the desulphurisation process, and
- to find alternative initial slag modifying agents based on a literature review.

A sampling campaign was organised in order to study the composition and amount of initial slag. During the sampling campaign, 10 initial slag samples were obtained. Unfortunately, the measurements of the thickness of the slag layer were not successful. In addition to the small number of samples, five of them had to be discarded due to high amounts of carbon and missing process data. However, the data was combined with previously collected samples, thus allowing a more representative dataset for subsequent analysis. The main conclusions made based on the dataset were:

- The amount of CaO in the slag phase increases as a function of the temperature of the bath before hot metal desulphurisation. Reasons for this are the wearing of skulls from the ladle at higher temperatures, and the exothermic reaction of the forming of the other main component of the slag, SiO_2. CaO increases the basicity of the slag, which is favourable for desulphurisation.
- The amount of Na_2O in the slag phase decreases as a function of temperature due to evaporation. While higher temperatures are advantageous for desulphurisation, the evaporation of Na_2O should also be considered.
- The amount of Fe entrapped within the slag decreases as a function of the addition of Na_2CO_3, which is currently used to fluidise the slag.
- According to the analysis, the sulphur distribution ratio increases as a function of the temperature, and CaO and Na_2O content of the slag, whereas the Mn in the slag seems to decrease it.

During the sampling campaign, a rapidly cooled piece of initial slag was obtained for microscopical study. The sample was studied utilising light optical microscopy (LOM) and field emission scanning electron microscopy (FESEM). The results and observations are summarised below:

- The structure of the cooled piece of initial slag was found to be dendritic, which is a result of the cooling of the sample.
- Based on the FESEM analyses, the main phase appeared to be a glassy phase with a composition close to that of melilite. However, no melilite had crystallised in the sample.
- Of the main phase, a larnite phase had started to crystallise before the sample had solidified. This indicates that the sample was thoroughly molten at the moment of sampling. Thus, it can be stated that the current initial slag modifying agent had induced the desired fluidising effect on the slag. Liquid slags are generally thought to be favourable for desulphurisation, although they may cause resulphurisation if the sulphide capacity of the slag is low.

An industrial test-run was conducted in order to test ladle slag (LS) as a new initial slag modifying agent. The effects of LS on the liquid fraction, dynamic viscosity and the sulphide capacity of the slag were studied beforehand. The predicted compositions of the LS-added initial slags with varying masses of both slags were calculated based on previous analyses of initial slag and LS, and the obtained compositions were used in the calculations. The results indicated that LS increases the liquid fraction and the sulphide capacity of the slag, and decreases the dynamic viscosity already at small additions, although the liquid fraction exhibited nonlinear behaviour at higher additions. Based on the study, the amount of LS was set to 50 kg per ladle.

The test-run was divided into two series: 1) LS addition, and 2) LS & Na_2CO_3 addition. At the moment of sampling, initial slag was observed to be molten throughout the test-run. Average desulphurisation efficiency during the test-run was 92%, which is 13% higher than during the sampling campaign. However, since samples were not collected from slags without the addition of LS during the test-run, it cannot be stated that the

higher desulphurisation efficiencies would be a result of the use of LS in initial slag modification.

The predicted compositions of the slags were compared to the measured compositions during the test-run. It was discovered that the amount of Fe entrapment was substantially lower than predicted, especially when LS alone was used. This result, combined with the observations of liquid slag during the test-run, indicate that LS had succeeded in fluidising the slag. After removing Fe and normalising the compositions, the compositions corresponded reasonably well to each other.

The average masses of initial slag of the two test series were estimated by minimising the SSE for predicting the compositions of the slags by changing the mass of initial slag before the addition of LS. The obtained estimates were 185.4 and 372.3 kg for series 1 and 2, respectively. In addition, the mass and origin of initial slag was studied based on analyses of the main constituents of initial slag. The SSE for predicting the composition of the initial slag was minimised by changing the masses of BF slag and skull in the ladle. The estimated average mass of initial slag after LS addition was 480.6 kg, and the average estimated contributions of the studied constituents of initial slag were 46.5 wt-% skull, 22.7 wt-% BF slag, and 12.8 wt-% SiO_2 originating from Si oxidised from the hot metal. In some experiments, the error was fairly small. However, in part of the experiments SiO_2 had reduced from the slag to the metal phase, according to the hot metal samples, thus leading to large errors in the predictions. It should also be noted that with respect to MgO, the estimated mass of BF slag reached higher values than theoretically possible in some experiments. This is due to MgO originating only from BF slag and LS; with higher amounts of BF slag, the amount of MgO in initial slag should also be higher. It was discovered that the amount of BF slag is smaller in the ladles that are filled first during the tapping of hot metal. This is most likely because of the fact that by that time the slag had not yet started to exit the BF.

The sulphide capacities of the slags were calculated for the whole dataset, including the sampling campaign combined with the previously collected samples, and the test-run. The results were compared to those obtained by utilising a model proposed by Young et al. (1992), which used the optical basicity concept for estimating the sulphide capacity.

It was discovered that the model did not perform well with the present dataset; thus, a novel model for predicting the sulphide capacity of the slag was constructed.

The effect of initial slag on the desulphurisation process was studied by utilising multi-variable linear regression (MVLR) models. The response variables of interest were the sulphide capacity of the slag, desulphurisation efficiency, and the amount of sulphur in hot metal after desulphurisation. Unfortunately, slag components did not exhibit statistical significance in the prediction models for S_{eff} and S_t or the sign of the regression coefficient was incorrect. Hence the attempt to elucidate the effect of initial slag on the desulphurisation process did not succeed. However, a novel model for predicting the sulphide capacity of the slag was constructed. The accuracy of the model was confirmed with this dataset ($R^2_{\text{adj.}} = 0.77$). The obtained equation for estimating the sulphide capacity of the slag is as follows:

$$\log_{10} C_S = 0.03323(Na_2O) + 0.01162(CaO) - 0.16779(Mn) + 0.0019T_0 - 6.74726, \quad (38)$$

where (Na_2O), (CaO) and (Mn) refer to the amount of Na_2O, CaO and Mn in the slag phase in wt-%, respectively, and T_0 is the temperature before hot metal desulphurisation.

11 REFERENCES

Abd Elmomen, S. S., 2017. Influence of Slag Composition and Temperature on Silicon Distribution between Slag and Hot Metal in the Egyptian Blast Furnace No.III. Journal of Petroleum and Mining Engineering 19 (1). P. 26–32.

Amini, S., Brungs, M. & Ostrovski, O., 2007. Dissolution of Dense Lime in Molten Slags under Static Conditions. ISIJ International 47 (1). P. 32–37.

Andersson, M. A. T., Jönsson, P. G., Hallberg, M., 2000. Optimisation of ladle slag composition by application of sulphide capacity model. Ironmaking & Steelmaking 27 (4). P. 286–293.

Babich, A., Senk, D., Gudenau, W. & Mavrommatis, K. T., 2008. Ironmaking. Aachen: Institut für Eisenhüttenkunde der RWTH Aachen, 402 p. ISBN 3-86130-997-1

Bakker, T., Husslage, W. M., Reuter, M. A., den Exter, P. & Steeghs, A. G. S., 2002. Hot metal quality: Always a hot topic. 61st Ironmaking Conference, Nashville, March, 2002, P. 241–254.

Ban-Ya, S., 1993. Mathematical Expression of Slag-Metal Reactions in Steelmaking Process by Ouadratic Formalism Based on the Regular Solution Model. ISIJ International 33 (1). P. 2–11.

Cao, Q., Nastac, L., Pitts-Baggett, A. & Yu, Q., 2018. Numerical Investigation of Desulfurization Kinetics in Gas-Stirred Ladles by a Quick Modeling Analysis Approach. Metallurgical and Materials Transactions B 49 (3). P. 988–1002.

Chan, A. H. & Fruehan, R. J., 1989. The Sulfur Partition Ratio with Fe-C_{SAT} Melts and the Sulfide Capacity of CaO-SiO_2-Na_2O-(Al_2O_3) Slags. Metallurgical Transactions B 20 (1). P. 71–76.

Chiang, L-K., 1986. A Kinetic Study of Hot Metal Desulfurization by Calcium Carbide Powder Injection [Doctoral Thesis]. Hamilton, Ontario: McMaster University. 327 P.

Chiang, L-K., Irons, G. A., Lu, W-K & Cameron, I. A., 1990. Kinetic Studies of Calcium Carbide Hot Metal Desulfurization by Powder Injection. Iron Steelmaker 17 (1). P. 35–52.

Cho, M. K., Cheng, J., Park, J. H. & Min, D. J., 2010. Hot Metal Desulfurization by CaO-SiO_2-CaF_2-Na_2O Slag Saturated with MgO. ISIJ International 50 (2). P. 215–221.

Choi, J. Y., Kim, D. J. & Lee, H. G., 2001. Reaction Kinetics of Desulfurization of Molten Pig Iron Using CaO-SiO_2-Al_2O_3-Na_2O Slag Systems. ISIJ International 41 (3). P. 216–224.

Chushao, X. & Xin, T., 1992. The Kinetics of Desulphurization of Hot Metal by CaO-CaF_2 based fluxes. ISIJ International 32 (10). P. 1081–1083.

Condo, A. F. T., 2018. Study of Sulfide Capacity of Slag and Sulfur Removal of Hot Metal [Doctoral thesis]. Stockholm: KTH Royal Institute of Technology. 52 P.

Diao, J., Xie, B. & Wang, S. S., 2009. Research on slag modifying agents for CaO-Mg based hot metal desulphurisation. Ironmaking & Steelmaking 36 (7). P. 543–547.

Deo, B. & Grieveson, P., 1988. Desulphurization of molten pig iron containing aluminium by powder injection. Steel Research 59 (6). P. 263–268.

Duffy, J. A. & Ingram, M. D., 1976. An interpretation of glass chemistry in terms of the optical basicity concept. Journal of Non-Crystalline Solids 21 (3). P. 373–410.

Halikia, I., Zoumpoulakis, L., Christodoulou, E. & Prattis, D., 2001. Kinetic study of the thermal decomposition of calcium carbonate by isothermal methods of analysis. The European Journal of Mineral Processing and Environmental Protection 1 (2). P. 89–102.

Holappa, L. E. K., 1980. Review of Ladle Metallurgy. Scandinavian Journal of Metallurgy 9 (6). P. 261–266.

Husslage, W., 2004. Dynamic distributions: Sulphur transfer and flow in a high temperature packed coke bed [Doctoral thesis]. 228 P.

Inoue, R. & Suito, H., 1982. Sulfur Partitions between Carbon-saturated Iron Melt and Na_2O-SiO_2 Slags. Transactions of the Iron and Steel Institute of Japan 22 (7). P. 514–523.

Irons, G. A., 1986. Fundamental and practical aspects of lance design for powder injection processes. 4th International Conference on Injection Metallurgy, Luleå, Sweden, June 11–13, 1986, Proceedings, Part 1, P. 3:1–25.

Irons, G. A., 1989. Role of mixing in powder injection desulphurisation processes. Ironmaking and Steelmaking 16 (1). P. 28–36.

Irons, G. A. & Farias, L. R., 1986. The influence of lance orientation and gas evolution on particle-liquid contact during submerged powder injection. Canadian Metallurgical Quarterly 25 (4). P. 297–306.

Jin, Y., Bi, X. G. & Yu, S. R., 2006. Kinetic Model for Powder Injection Desulfurization. Acta Metallurgica Sinica (English Letters) 19 (4). P. 258–264.

Jussi Hulkkonen. 22.10.2009. (internal report)

Kanyangarara, M. T., 1982. Desulphurisation of iron by slags [Doctoral thesis]. London: University of London. 158 P.

Kingston, P. W. & Caley, W. F., 1989. Nepheline syenite as a synthetic slag addition in secondary steelmaking. Minerals Engineering 2 (2). P. 207–215.

Kitamura, S. Y., 2014. Chapter 1.3 – Hot metal pretreatment. In: Seetharaman, S. Treatise on Process Metallurgy. Volume 3: Industrial Processes. Elsevier, P. 177–221. ISBN 978-0-08-096988-6

Li, M., Utigard, T. & Barati, M., 2015. Kinetics of Na_2O and B_2O_3 Loss From CaO-SiO_2-Al_2O_3 Slags. Metallurgical and Materials Transactions B 46 (1). P. 74–82.

Magnelöv, M., Eriksson, J., Drugge, J., Björkvall, J. & Björkman, B., 2013. Investigation of iron losses during desulphurisation of hot metal utilising nepheline syenite. Ironmaking and Steelmaking 40 (6). P. 436–442.

Montgomery, D. C., Peck, E. A. & Vining, G. G., 2012. Introduction to Linear Regression Analysis (5th Edition). Hoboken, New Jersey: John Wiley & Sons Inc, 645 p. ISBN 978-0-470-54281-1

Moosavi-Khoonsari, E. & Jung, I. H., 2016. Thermodynamic Modeling of Sulfide Capacity of Na_2O-Containing Oxide Melts. Metallurgical and Materials Transactions B 47 (5). P. 2875–2888.

Næss, M. K., 2013. Mechanisms and kinetics of liquid silicon oxidation [Doctoral thesis]. Trondheim: Norwegian University of Science and Technology. 105 P.

O'Brien, R. M., 2007. A Caution Regarding Rules of Thumb for Variance Inflation Factors. Quality & Quantity 41 (5). P. 673–690.

Ohguchi, S., 1983. Accretion growth and slag-metal reactions in injection metallurgy [Doctoral thesis]. London: Imperial College of Science and Technology. 232 P.

Oeters, F., 1985. Kinetic treatment of chemical reaction in emulsion metallurgy. Steel research 56 (2). P. 69–74.

Pak, J. J. & Fruehan, R. J., 1987. Dynamics of the Hot Metal Dephosphorization with Na_2O Slags. Metallurgical Transactions B 18 (4). P. 687–693.

Pal, U. B. & Patil, B. V., 1986. Role of dissolved oxygen in hot metal desulphurization. Ironmaking and Steelmaking 13 (6). P. 294–300.

Palovaara, P., 2013. Raakaraudan rikinpoiston roiskumisen hallinta [Master's thesis]. Oulu: University of Oulu. 157 P.

Petri Palovaara. 10.9.2012. (internal report)

Polychronopoulou, A., Pandis, N. & Eliades, T., 2011. Appropriateness of reporting statistical results in orthodontics: the dominance of P values over confidence intervals. European Journal of Orthodontics 33 (1). P. 22–25.

Rawlings, J. O., Pantula, S. G. & Dickey, D. A., 1998. Applied Regression Analysis: A Research Tool (2nd Edition). New York: Springer-Verlag New York, Inc., 634 p. ISBN 0-387-98454-2

Sano, N., 2003. Improvement of Refining Capacities of CaO based Slags by a Small Addition of Na_2O. High Temperature Materials and Processes 22 (5–6). P. 353 – 358.

Sawada, I., Kitamura, T., & Ohashi, T., 1986. The Mathematical Modelling of the Coupled Reactions in the Pre-treatment of Molten Iron by Powder Injection. Scaninject IV, 1986.

Schrama, F. N., Beunder, E. M., Van der Berg, B., Yang, Y. & Boom, R., 2017. Sulphur removal in ironmaking and oxygen steelmaking. Ironmaking & Steelmaking, 44 (5), P. 333–343.

Schrama, F. N. H., Moosavi-Khoonsari, E., Beunder, E. M., Kooij, C., Boom, R., Sietsma, J. & Yang, Y, 2018a. Slag optimisation considering iron loss and sulphide capacity in hot metal desulphurisation. in ICS 2018 – 7th International Congress on Science and Technology of Steelmaking: The Challenge of Industry 4.0. Associazione Italiana di Metallurgia, 7th International Congress on Science and Technology of Steelmaking, ICS 2018, Venice, Italy, 13.06.18.

Schrama, F. N. H., Beunder, E. M., Ji, F., Woolf, R., Barnes, C., Sietsma, J., Boom, R. & Yang, Y., 2018b. Effect of $KAlF_4$ on the efficiency of hot metal desulphurisation with magnesium. in 8th European Oxygen Steelmaking Conference, EOSC 2018, Taranto, Italy, 10.–12.10.2018.

Shevchenko, A. F., Kiyashko, A. G. & Mal'kov, A. N., 1984. Influence of particle size of lime on effectiveness of pig iron desulphurization. Steel In The USSR 14 (3). P. 116–117.

Sigworth, G. K. & Elliott, J. F., 1974. The Thermodynamics of Liquid Dilute Iron Alloys. Metal Science 8. P. 298–310.

Sosinsky, D. J. & Sommerville, I. D., 1986. The Composition and Temperature Dependence of the Sulfide Capacity of Metallurgical Slags. Metallurgical Transactions B 17 (2). P. 331–337.

SSAB, 2015. (internal brochure)

Tong, Z., Qiao, J. & Jiang, X., 2017. Hot Metal Desulphurization Kinetics by CaO–Al_2O_3–SiO_2–MgO–TiO_2–Na_2O Slags. ISIJ International 57 (2). P. 245–253.

Tribe, T. S., Kingston, P. W., MacDonald, J. B. & Caley, W. F., 1994. Reduction of fluorspar consumption in secondary steelmaking. Ironmaking and Steelmaking 21 (2). P. 145–149.

Turkdogan, E. T., 1996. Fundamentals of Steelmaking. London: The Institute of Materials, 331 p. ISBN 978-1-906540-97-5

Van Niekerk, W. H. & Dippenaar, R. J., 1993. Thermodynamic Aspects of Na_2O and CaF_2 Containing Lime-based Slags Used for the Desulphurization of Hot-metal. ISIJ International 33 (1). P. 59–65.

Varanasi, S. S., Pathak, R. K., Sahoo, K., K., More, V. M. R., Santanu, D. & Alli, S. R., 2019. Effect of CaO–Al_2O_3-Based Synthetic Slag Additions on Desulphurisation

Kinetics of Ladle Furnace Refining. Transactions of the Indian Institute of Metals 72 (6). P. 1447–1452.

Vargas-Ramirez, M., Romero-Serrano, A., Morales, R., Angeles-Hernandez, M., Chavez-Alcala, F. & Castro-Arellano, J., 2001. Hot metal pretreatment by powder injection of lime-based reagents. Steel Research 72 (5+6). P. 173–181.

Vasilopoulos, A., 2011. Hypothesis Testing: A Statistical Procedure for Testing the Validity of Claims. In: Tomic, M. Review of business. St. John's University, P. 89–110. ISSN: 0034-6454

Visuri, V-V., Sulasalmi, P., Vuolio, T., Haas, T., Hay, T., Pfeifer, H., Paananen, T. & Fabritius, T., 2019. A Mathematical Model for Hot Metal Desulfurization: Derivation of the Model. Unpublished manuscript.

Vuolio, T., 2017. Improvement Potential Of Primary Hot Metal Desulphurization [Master's thesis]. Oulu: University of Oulu. 162 P.

Vuolio, T., Visuri, V-V., Tuomikoski, S., Paananen, T. & Fabritius, T., 2018. Data-Driven Mathematical Modeling of the Effect of Particle Size Distribution on the Transitory Reaction Kinetics of Hot Metal Desulphurisation. Metallurgical and Materials Transactions B 49 (5). P. 2692–2708.

Vuolio, T., Visuri, V-V., Paananen, T. & Fabritius, T., 2019. Identification of Rate, Extent, and Mechanisms of Hot Metal Resulfurization with CaO-SiO_2-Na_2O Slag Systems. Metallurgical and Materials Transactions B 50 (4). P. 1791–1807.

Walker, D. C., 2010. Modification of Steelmaking Slag by Additions of Salts from Aluminium Production [Master's thesis of applied science]. Halifax, Nova Scotia: Dalhousie University. 77 P.

Wang, L., Wu, S., Kou, M., Du, B., Lu, Y. & Gu, K., 2018. Improving the Desulphurization in COREX Process by Adjusting the Hot Metal Chemical Composition. Metallurgical and Materials Transactions B 49 (1). P. 89–97.

Willmott, C. J., Matsuura, K., 2005. Advantages of the mean absolute error (MAE) over the root mean square error (RMSE) in assessing average model performance. Climate research 30 (1). P. 79–82.

Wolfe, L. & Olson, L., 2003. Yield Improvements During Iron Desulphurisation When Utilizing "Flow Aided" Compounds for Modifying Slag Characteristics [web document]. Iron & Steel Society International Technology Conference and Exposition 2003 (p. 369-378). [accessed 3.5.2019].

Wu, S., Wang, L., Lu, Y. & Gu, K., 2018. Improving the Desulphurization in COREX-3000 Process by the Optimization of Chemical Compositions of Slag. ISIJ International 58 (11). P. 2025–2031.

Yang, A. F., Karasev, A. & Jönsson, P. G., 2016. Effect of Nepheline Syenite on Iron Losses in Slags during Desulphurization of Hot Metal. Steel Research International 87 (5). P. 599–607.

Young, R. W., Duffy, J. A., Hassall, G. J. & Xu, Z., 1992. Use of optical basicity concept for determining phosphorus and sulphur slag–metal partitions. Ironmaking and Steelmaking 19 (3). P. 201–219.

Zhang, K., Zhang, Y. & Wu, T., 2018. Distribution Ratio of Sulfur between CaO-SiO_2-Al_2O_3-Na_2O-TiO_2 Slag and Carbon-Saturated Iron. Metals 2018 8 (12), 1068.

Zhao, Y., 1992. The role of oxygen in hot metal desulphurization with calcium carbide powder injection [Doctoral thesis]. Hamilton, Ontario: McMaster University. 338 P.

Zhou, S. C., 2012. Effect of B_2O_3 on the melting temperature and viscosity of desulphurization slag in V-Ti bearing hot metal. Metallurgia international XVII (9). P. 230–233.

Zhu, C-Y., Chen, P-J., Li, Q-Q., Luo, X-Y. & Zheng, W., 2016. A Mathematical Model of Desulphurization Kinetics for Ultra-low-sulfur Steels Refining by Powder Injection during RH Processing. ISIJ International 56 (8). P. 1368–1377.

Analyses of the slag samples in wt-%

Sample	T (°C)	m_{HM} (t)	Reag. (kg)	K_2O	Na_2O	C	S	MgO	Al_2O_3	SiO_2	CaO	Ti	Mn	Fe	FeM05
D1S1 (before)	1272	81.98	1315	0.061	17.9	0.81	1.25	0.1	0.5	7.1	0.86	0.29	0.88	84	75.4
D1S2 (before)	1467	80.73	967	0.050	4.57	0.04	1.18	1.2	6.6	31.8	40.7	1.6	0.51	11.9	6.9
D1S3 (before)	1276	N/A	N/A	0.108	11.4	0.70	2.38	0.51	0.73	9.9	7.3	0.76	0.32	76	70.9
D2S2 (before)	1386	82.86	1081	0.074	14.6	12	2.20	0.82	4	20.6	16.1	1.3	0.37	40	34.9
D2S3 (before)	1378	81.59	816	0.055	19.2	4.5	1.65	0.88	2.7	30.5	17.3	1.8	0.46	26.6	21.5
D2S4 (before)	1425	73.72	815	0.043	6.26	28	0.542	0.23	2.5	7.4	2.2	1.3	0.57	70.4	60.2
D2S5 (before)	1332	85.15	982	0.262	16.5	18	1.24	0.13	0.65	8.4	0.42	0.55	0.17	79	75.5
D3S1 (before)	1311	79.42	1216	0.194	8.29	1.7	0.778	0.3	5	15.9	7.2	1.6	3.3	55.3	40.7
D3S2 (before)	1442	82.00	967	0.066	17.5	0.14	2.79	1.2	4.7	28.4	32.8	1.5	1.1	14.6	10.9
D3S3 (before)	1345	80.53	1265	0.123	21.6	1.4	1.04	0.55	3.3	23.2	8.1	2.7	3.1	39.1	28.4

Sample	T (°C)	m_{HM} (t)	Reag. (kg)	K_2O	Na_2O	C	S	MgO	Al_2O_3	SiO_2	CaO	Ti	Mn	Fe	FeM05
S1E1 (before)	1434	79.78	947	0.099	1.08	0.02	0.651	2.4	10.9	37.5	37.2	2.4	1.5	4.39	0.5
S1E2 (before)	1416	88.63	1092	0.083	13.1	0.06	2.80	1.9	12.2	31	29	1.8	0.71	10.7	7.8
S1E3 (before)	1404	80.68	1062	0.097	3.05	0.02	1.58	1.3	6.1	34.2	44.7	2.3	0.97	6.76	3.3
S1E4 (before)	1360	83.09	1046	0.125	14.5	0.07	1.46	2	9.8	38.4	26.5	2.8	1.2	3.95	1.4
S1E5 (before)	1396	82.33	1142	0.076	2.13	0.03	1.43	1.8	7.4	32.6	42.2	2	0.88	10.3	6.7
S1E6 (before)	1429	81.56	1083	0.074	0.714	0.14	0.623	2.3	10.1	31.6	31	2	1.4	18.3	11.9
S1E7 (before)	1385	85.46	829	0.062	0.427	0.24	0.678	1.9	7.5	28.6	27.5	1.8	1.3	28	19.6
S2E1 (before)	1424	84.90	1185	0.123	10.5	0.04	1.67	2.4	11.1	33.6	34	1.9	0.79	5.51	1.3
S2E2 (before)	1395	81.29	1000	0.067	19.0	0.08	4.09	1.7	8.4	34.1	30.3	2.1	0.46	2.64	0.4
S2E3 (before)	1399	83.08	1039	0.054	12.1	0.06	2.02	2.1	8.3	34.3	35.5	2	0.73	5.54	1.6
S2E4 (before)	1416	75.95	1158	0.121	12.8	0.04	1.86	3.2	10.4	36.1	32.7	2.1	0.68	3.29	0.7
S2E7 (before)	1362	81.84	863	0.079	8.57	0.05	2.03	1.7	6.5	31.5	34.3	1.9	0.65	14.7	11.6
S2E8 (before)	1412	83.09	915	0.053	12.5	0.08	2.74	2.3	8	30.9	33.1	2	0.85	11	6.3

Sample	T (°C)	m_{HM} (t)	Reag. (kg)	K_2O	Na_2O	C	S	MgO	Al_2O_3	SiO_2	CaO	Ti	Mn	Fe	FeM05
S1E1 (after)	1393	79.78	947	0.035	2.03	1.0	2.44	0.7	1.4	8.4	40.2	0.38	0.16	40.2	25.8
S1E2 (after)	1373	88.63	1092	0.031	3.48	0.18	4.67	0.9	3	11.9	48.8	0.64	0.19	21.2	14.0
S1E3 (after)	1363	80.68	1062	0.060	2.65	1.2	1.46	0.46	0.69	4.8	27.4	0.24	0.11	56.3	43.9
S1E4 (after)	1332	83.09	1046	0.034	1.83	0.97	2.47	0.54	0.98	6.2	32	0.31	0.15	51.5	38.2
S1E5 (after)	1361	82.33	1142	0.033	2.01	0.72	2.25	0.7	1.6	8.5	38.5	0.4	0.17	36.3	25.3
S1E6 (after)	1382	81.56	1083	0.031	1.83	0.74	2.68	0.69	2.2	10	38.6	0.41	0.16	40.5	29.2
S1E7 (after)	1355	85.46	829	0.037	1.54	1.3	1.38	0.36	0.36	3.6	24.4	0.16	0.11	61.7	44.9
S2E1 (after)	1381	84.90	1185	0.045	3.52	0.64	2.72	1	2.5	10.8	47.4	0.48	0.16	22.9	14.4
S2E2 (after)	1363	81.29	1000	0.043	2.26	1.6	0.678	0.36	0.53	2.6	22.9	0.09	0.06	63.1	45.8
S2E3 (after)	1368	83.08	1039	0.033	3.79	0.41	2.26	0.89	1.9	11	43.5	0.48	0.16	28.3	20.2
S2E4 (after)	1373	75.95	1158	0.029	2.90	0.27	2.17	0.98	2	9.4	45.5	0.41	0.12	29.9	22.7
S2E5 (after)	1361	85.73	914	0.039	2.79	0.97	2.53	0.65	1.7	7.4	36.7	0.35	0.14	43.6	29.1
S2E6 (after)	1378	81.29	1020	0.044	3.01	0.71	2.55	0.78	1.5	10	43.5	0.38	0.14	33.9	17.3
S2E7 (after)	1335	81.84	863	0.071	3.29	1.3	1.36	0.48	0.8	5.8	28.8	0.28	0.13	53	39.2
S2E8 (after)	1376	83.09	915	0.089	3.66	2.2	0.605	0.58	0.41	2.3	38.3	0.091	0.07	35.5	19.8

Analyses of the hot metal samples in wt-%

Sample	T (°C)	m_{HM} (t)	Reag. (kg)	C	S	Si	P	Ti	V	Cr	Mn	Ni	Cu	Zn
D1S1 (before)	1272	81.98	1315	3.54	0.1845	0.087	0.045	0.009	0.162	0.030	0.075	0.027	0.007	0.002
D1S2 (before)	1467	80.73	967	4.64	0.0461	0.647	0.051	0.095	0.256	0.040	0.217	0.028	0.008	0.003
D1S3 (before)	1276	N/A	N/A	3.90	0.1550	0.273	0.050	0.040	0.200	0.036	0.125	0.027	0.007	0.002
D2S1 (before)	1340	78.10	913	4.57	0.0482	0.843	0.053	0.102	0.260	0.035	0.198	0.029	0.006	0.003
D2S2 (before)	1386	82.86	1081	4.64	0.0530	1.040	0.054	0.122	0.279	0.035	0.205	0.028	0.006	0.002
D2S3 (before)	1378	81.59	816	4.68	0.0352	0.866	0.053	0.122	0.264	0.035	0.207	0.029	0.006	0.002
D2S4 (before)	1425	73.72	815	4.75	0.0344	1.020	0.055	0.134	0.268	0.043	0.711	0.030	0.008	0.003
D2S5 (before)	1332	85.15	982	4.61	0.0464	0.745	0.052	0.095	0.261	0.035	0.186	0.028	0.008	0.003
D3S1 (before)	1311	79.42	1216	4.50	0.0664	0.593	0.053	0.065	0.242	0.042	0.645	0.029	0.009	0.004
D3S2 (before)	1442	82.00	967	4.56	0.0411	0.608	0.052	0.077	0.240	0.041	0.631	0.029	0.008	0.003
D3S3 (before)	1345	80.53	1265	4.47	0.0587	0.565	0.051	0.064	0.235	0.040	0.615	0.029	0.009	0.003
D1S1 (after)	1247	81.98	1315	3.49	0.0144	0.022	0.043	0.003	0.165	0.031	0.066	0.029	0.006	0.001
D1S2 (after)	1421	80.73	967	4.59	0.0055	0.598	0.052	0.095	0.254	0.040	0.218	0.029	0.007	0.003
D1S3 (after)	1256	N/A	N/A	3.90	0.0111	0.165	0.051	0.016	0.200	0.037	0.118	0.027	0.007	0.002
D2S1 (after)	1304	78.10	913	4.51	0.0108	0.793	0.054	0.094	0.260	0.036	0.197	0.029	0.007	0.003
D2S2 (after)	1352	82.86	1081	4.59	0.0077	0.973	0.055	0.120	0.279	0.036	0.204	0.028	0.007	0.002
D2S3 (after)	1348	81.59	816	4.61	0.0104	0.817	0.053	0.119	0.263	0.036	0.208	0.028	0.006	0.002
D2S4 (after)	1389	73.72	815	4.69	0.0073	0.988	0.056	0.132	0.267	0.043	0.707	0.031	0.008	0.002
D2S5 (after)	1299	85.15	982	4.52	0.0094	0.690	0.052	0.090	0.260	0.036	0.186	0.029	0.007	0.002
D3S1 (after)	1272	79.42	1216	4.48	0.0071	0.512	0.053	0.059	0.244	0.042	0.652	0.030	0.009	0.003
D3S2 (after)	1395	82.00	967	4.54	0.0048	0.582	0.053	0.076	0.239	0.042	0.633	0.029	0.008	0.003
D3S3 (after)	1313	80.53	1265	4.47	0.0043	0.494	0.051	0.061	0.235	0.040	0.616	0.030	0.009	0.003

Sample	T (°C)	m_{HM} (t)	Reag. (kg)	C	S	Si	P	Ti	V	Cr	Mn	Ni	Cu	Zn
S1E1 (before)	1434	79.78	947	4.56	0.0643	0.419	0.054	0.077	0.289	0.045	0.234	0.033	0.009	0.001
S1E2 (before)	1416	88.63	1092	4.55	0.0769	0.402	0.055	0.068	0.278	0.044	0.216	0.032	0.009	0.001
S1E3 (before)	1404	80.68	1062	4.53	0.0740	0.377	0.056	0.067	0.294	0.046	0.227	0.033	0.008	0.002
S1E4 (before)	1360	83.09	1046	4.40	0.0551	0.342	0.055	0.058	0.285	0.045	0.239	0.034	0.008	0.001
S1E5 (before)	1396	82.33	1142	4.41	0.0522	0.365	0.056	0.063	0.297	0.047	0.255	0.033	0.009	0.002
S1E6 (before)	1429	81.56	1083	4.53	0.0543	0.384	0.056	0.069	0.292	0.045	0.237	0.033	0.008	0.002
S1E7 (before)	1385	85.46	829	4.52	0.0587	0.460	0.055	0.080	0.300	0.046	0.238	0.033	0.009	0.001
S2E1 (before)	1424	84.90	1185	4.66	0.0545	0.440	0.052	0.079	0.266	0.042	0.224	0.032	0.008	0.001
S2E2 (before)	1395	81.29	1000	4.71	0.0405	0.557	0.054	0.096	0.288	0.044	0.235	0.033	0.008	0.001
S2E3 (before)	1399	83.08	1038	4.55	0.0369	0.370	0.054	0.070	0.295	0.045	0.251	0.032	0.009	0.001
S2E4 (before)	1416	75.95	1158	4.58	0.0395	0.387	0.054	0.075	0.274	0.043	0.233	0.033	0.009	0.001
S2E5 (before)	1389	85.73	914	4.59	0.0600	0.442	0.053	0.079	0.272	0.043	0.210	0.033	0.009	0.002
S2E6 (before)	1420	81.29	1020	4.71	0.0518	0.477	0.054	0.091	0.285	0.044	0.233	0.033	0.008	0.001
S2E7 (before)	1362	81.84	863	4.58	0.0540	0.343	0.053	0.067	0.292	0.045	0.240	0.033	0.008	0.001
S2E8 (before)	1412	83.09	915	4.62	0.0643	0.779	0.052	0.065	0.263	0.042	0.213	0.033	0.009	0.001

Sample	T (°C)	m_{HM} (t)	Reag. (kg)	C	S	Si	P	Ti	V	Cr	Mn	Ni	Cu	Zn
S1E1 (after)	1393	79.78	947	4.56	0.0034	0.383	0.054	0.073	0.287	0.045	0.235	0.033	0.008	0.001
S1E2 (after)	1373	88.63	1092	4.46	0.0042	0.393	0.055	0.062	0.278	0.044	0.218	0.033	0.009	0.001
S1E3 (after)	1363	80.68	1062	4.41	0.0045	0.293	0.056	0.054	0.286	0.045	0.241	0.034	0.008	0.001
S1E4 (after)	1332	83.09	1046	4.48	0.0036	0.330	0.057	0.062	0.293	0.046	0.226	0.033	0.009	0.001
S1E5 (after)	1361	82.33	1142	4.41	0.0026	0.295	0.056	0.059	0.297	0.046	0.257	0.033	0.008	0.001
S1E6 (after)	1382	81.56	1083	4.45	0.0038	0.413	0.057	0.066	0.291	0.045	0.238	0.033	0.008	0.001
S1E7 (after)	1355	85.46	829	4.49	0.0093	0.401	0.055	0.074	0.299	0.046	0.239	0.033	0.008	0.001
S2E1 (after)	1381	84.90	1185	4.66	0.0033	0.395	0.053	0.075	0.265	0.042	0.223	0.033	0.009	0.001
S2E2 (after)	1363	81.29	1000	4.75	0.0028	0.491	0.055	0.098	0.288	0.044	0.237	0.033	0.008	0.000
S2E3 (after)	1368	83.08	1038	4.49	0.0039	0.331	0.055	0.067	0.294	0.045	0.251	0.033	0.009	0.001
S2E4 (after)	1373	75.95	1158	4.55	0.0022	0.340	0.054	0.072	0.274	0.044	0.235	0.033	0.009	0.001
S2E5 (after)	1361	85.73	914	4.57	0.0071	0.387	0.053	0.075	0.272	0.042	0.212	0.033	0.009	0.001
S2E6 (after)	1378	81.29	1020	4.58	0.0013	0.417	0.053	0.085	0.280	0.044	0.229	0.032	0.008	0.000
S2E7 (after)	1335	81.84	863	4.47	0.0055	0.291	0.053	0.062	0.293	0.046	0.237	0.033	0.009	0.001
S2E8 (after)	1376	83.09	915	4.58	0.0060	0.324	0.053	0.062	0.264	0.042	0.213	0.033	0.009	0.001